https://doi.org/10.5194/essd-2025-682
Preprint. Discussion started: 9 March 2026

Open Access Earth System Science Data Discussions

GloSVeT: a global 0.05 ° monthly mean surface soil and vegetation component temperature dataset (2003–2023)

Xiangyang Liu[1], Zhao-Liang Li[1,2], Chen Ru[1], Si-Bo Duan[1], Pei Leng[1]

[1]State Key Laboratory of Efficient Utilization of Arid and Semi-arid Arable Land in Northern China, Institute of Agricultural Resources and Regional Planning, Chinese Academy of Agricultural Sciences, Beijing 100081, China
[2] State Key Laboratory of Resources and Environment Information System, Institute of Geographic Sciences and Natural Resources Research, Chinese Academy of Sciences, Beijing 100101, China

Correspondence to: Zhao-Liang Li (lizhaoliang@caas.cn)

Abstract. Current satellite-derived land surface temperature products represent a mixed radiative signal that integrates soil and vegetation contributions, obscuring the physical mechanisms controlling surface energy partitioning and ecosystem functioning. To overcome this limitation, this study developed the Global Soil and Vegetation Temperature dataset (GloSVeT), the first global product that simultaneously provides surface soil and vegetation component temperatures at 0.05 ° spatial resolution for the period 2003–2023. GloSVeT was generated using the FuSVeT method, which integrates multi-temporal MODIS observations with ERA5-Land reanalysis to improve spatial completeness, retrieval accuracy, and computational efficiency. Its performance was extensively assessed through a comprehensive evaluation framework combining flux-tower validation, triple collocation (TC) analysis, and physical consistency assessments. Results show that GloSVeT achieves high accuracy, with coefficients of determination exceeding 0.9 and root mean square errors around 2 K for both components. TC analysis further demonstrates globally consistent performance, with distinct advantages in humid tropics and transitional ecosystems compared with reanalysis products. In addition, soil temperature anomalies correlate negatively with soil moisture whereas vegetation temperature aligns with solar-induced fluorescence along a clear gradient from energy-limited to water-limited biomes, indicating the physical realism of GloSVeT. Both components exhibit significant warming during 2003–2023 (0.39–0.44 K/decade), with spatially and seasonally interpretable patterns. In summary, GloSVeT provides a physically consistent, observation-driven depiction of surface thermal dynamics, offering new opportunities for quantifying land–atmosphere energy exchange, monitoring ecosystem hydrothermal responses, and improving the representation of land surface processes in Earth system models. GloSVeT is publicly available at https://doi.org/10.5281/zenodo.17461084, and https://data.tpdc.ac.cn/zh-hans/data/13b88dce-6bea-45f6-90e6-136e1fb57768.

1 Introduction

Land surface temperature (LST) is a key boundary variable governing the exchange of energy and water between the land surface and the atmosphere (Li et al., 2023). It captures a broad range of surface and ecological processes, including plant physiological activity and soil moisture dynamics (Li et al., 2021; Prentice et al., 2024), and has been widely applied in

https://doi.org/10.5194/essd-2025-682
Preprint. Discussion started: 9 March 2026

drought monitoring, urban heat island assessment, climate change analysis, and ecosystem modeling (Blyth et al., 2021; Wan et al., 2021; Wang et al., 2025). However, satellite-based LST products, owing to their limited spatial resolution, generally represent a mixed radiometric signal that combines temperature contributions from multiple components within each pixel (Li et al., 2013). This mixture obscures the heterogeneity of surface thermal conditions and constrains our understanding of how different land components, particularly soil and vegetation, regulate surface energy and water fluxes. In contrast, separating LST into soil and vegetation component temperatures provides a more physical and mechanistic representation of land–atmosphere interactions (Liu et al., 2020b; Zhan et al., 2013). Component temperature datasets thus serve as essential inputs for two-source energy balance modeling (Song et al., 2020), evapotranspiration partitioning (Jiang et al., 2022), vegetation stress diagnosis (Doughty et al., 2023), and studies of climate–ecosystem coupling (García-García et al., 2023).

Over the past decades, considerable efforts have been made to estimate soil temperature at global and regional scales. Reanalysis products such as ERA5-Land (Muñoz-Sabater et al., 2021) and GLDAS (Rodell et al., 2004), which rely on data assimilation techniques, provide soil temperature information at multiple depths and temporal scales with long-term continuity and seamless spatial coverage. However, their spatial resolution remains relatively coarse (typically 0.10 °–0.25 °). With the recent advances in artificial intelligence and the expansion of in situ observational networks, several machine learning–based soil temperature datasets have been developed (Baumberger et al., 2024; Lembrechts et al., 2022; Zhang et al., 2022). These datasets often achieve higher spatial resolutions, such as 1 km, but are generally limited in regional coverage (Baumberger et al., 2024; Zhang et al., 2022) or represent only climatological averages (Lembrechts et al., 2022), which constrains their broader applicability. Moreover, neither reanalysis nor machine learning products can accurately characterize the spatial pattern of soil thermal conditions in the real world. In contrast to soil temperature, no operational global product currently exists for vegetation temperature. In regions with dense vegetation cover, air temperature is often used as a proxy because of its strong coupling with canopy temperature (Li et al., 2001; Rutter et al., 2023; Zhan et al., 2011), while some studies have directly substituted LST for vegetation temperature when deriving vegetation physiological parameters such as evapotranspiration (Ma et al., 2022) or gross primary productivity (GPP) (Sims et al., 2008; Tang et al., 2021). Consequently, there still remains a lack of long-term, high-resolution datasets that simultaneously provide soil and vegetation component temperatures over the same regions under diverse environmental conditions.

Component temperature separation, which decomposes the LST of a single pixel into the temperatures of its constituent land surface components (Zhan et al., 2013), provides an effective pathway toward constructing such a dataset. Methodologically, this process involves solving an ill-posed problem, i.e., estimating soil and vegetation component temperatures from only one retrieved LST. Accordingly, a variety of algorithms have been developed to exploit additional temporal (Zhao et al., 2014), spatial (Song et al., 2015; Zhan et al., 2011), angular (Li et al., 2001; Lu et al., 2025), or spectral (Lundquist et al., 2018) information from satellite observations. Given the inherent limitations of each individual approach, several hybrid methods (Bian et al., 2020; Liu et al., 2020b) have been proposed to make full use of the complementary advantages of different types of information, advancing component temperature retrieval from theoretical algorithm development toward practical large-scale implementations. To further overcome the observational constraints of satellite data, Liu et al., (2025)

https://doi.org/10.5194/essd-2025-682
Preprint. Discussion started: 9 March 2026

developed a multisource data Fusion-based global surface Soil and Vegetation Temperature retrieval (FuSVeT) method, which integrates multi-temporal MODIS observations to increase the number of equations and incorporates ERA5-Land reanalysis data to reduce the unknown parameters. As a result, the FuSVeT framework delivers higher retrieval accuracy, more complete spatial coverage, and markedly improved computational efficiency compared with previous satellite-only approaches, providing a promising foundation for producing long-term global soil and vegetation component temperature datasets.

A further challenge in producing reliable component temperature products lies in the lack of effective validation strategies. Widely used ground-based measurement networks, such as the Surface Radiation Budget Network (SURFRAD, https://www.esrl.noaa.gov/gmd/grad/surfrad/), the AmeriFlux network (https://ameriflux.lbl.gov/) and the Karlsruhe Institute of Technology stations (KIT, https://www.imkasf.kit.edu/english/skl_stations.php), generally record either surface skin or air temperature rather than distinct soil and canopy components (He et al., 2025). Consequently, pixel-scale observations of soil and vegetation temperatures are extremely scarce, making direct evaluation of satellite-derived results nearly impossible. Some studies have attempted to identify pure pixels from higher-resolution satellite data and used their LSTs as reference values to assess coarse-resolution retrievals (Liu et al., 2025; Liu et al., 2020a). However, due to the sparse distribution of pure pixels, such localized comparisons cannot provide a comprehensive or statistically robust evaluation at continental or global scales. Examination of the spatiotemporal coherence of other temperature products, for instance through spatial gradients or temporal variation trends (Liu et al., 2025; Zhang et al., 2022), offers an alternative means of cross-validation, but these approaches generally yield only qualitative assessments. In contrast, robust non-reference validation frameworks have been developed to evaluate dataset reliability without relying on absolute ground truth. Among them, the triple collocation (TC) (Gruber et al., 2016; Park et al., 2023; Stoffelen 1998; Wei et al., 2024) and generalized three-cornered hat (TCH) (Premoli and Tavella 1993; Sjoberg et al., 2021) methods provide practical tools for quantifying the relative errors and mutual consistency among multiple independent datasets. Although originally designed for other geophysical variables such as soil moisture and precipitation, these methods have recently been extended to temperature-related datasets, i.e., monthly mean LST (Duan et al., 2024). Their demonstrated robustness and scalability make them particularly promising for evaluating component temperature products, offering a pathway toward large-scale, physically consistent assessments of spatiotemporal stability, internal coherence, and overall applicability.

To address these challenges, this study presents GloSVeT, the first global dataset of monthly mean surface soil and vegetation component temperatures from 2003 to 2023 at 0.05 ° spatial resolution. The dataset is generated using the previously developed FuSVeT framework, which has been adapted for global implementation through multi-source integration and large-scale automated processing. A systematic evaluation is conducted to examine the accuracy and reliability of GloSVeT through multiple complementary approaches, including site-based validation against in-situ temperature observations from a comprehensive network, TC analysis incorporating reanalysis soil and air temperatures, indicator-based consistency assessment with soil moisture and solar-induced fluorescence (SIF), and examination of seasonal spatiotemporal consistency. The results demonstrate that GloSVeT exhibits high accuracy, strong internal coherence, and

https://doi.org/10.5194/essd-2025-682
Preprint. Discussion started: 9 March 2026

stable temporal behaviour across diverse environmental conditions. As the first long-term, high-resolution global product that simultaneously represents soil and vegetation component temperatures, GloSVeT provides a valuable foundation for quantifying land–atmosphere energy exchange, partitioning evapotranspiration, and improving ecosystem and climate models. The dataset is freely available at https://doi.org/10.5281/zenodo.17461084.

2 Data

2.1 Data used for GloSVeT generation

To generate the GloSVeT, multiple datasets from satellite observations and reanalysis products were jointly employed to provide thermal, structural, and ancillary information (Table 1). These inputs ensure the physical consistency and global completeness of the GloSVeT production framework.

Variable	Dataset	Spatial Resolution	Temporal Resolution	Period	Purpose
Land surface temperature	MOD11C3/ MYD11C3	0.05 °	Monthly	2003–2023	Input thermal observations for constructing the separation model
Skin temperature	ERA5-Land	0.10 °	Hourly / Monthly mean	2003–2023	Model parameter simplification and constraint
Fractional vegetation cover	GLASS FVC	0.05 °	8-day	2003–2023	Pixel-scale structural parameterization for decomposition
Land cover	MCD12C1	0.05 °	Yearly	2003-2023	Masking of non-vegetated areas (water bodies and snow/ ice)

Table 1. Data used for the generation of the GloSVeT product

The long-term MODIS record provides more than two decades of globally consistent observations, making it one of the most widely used and physically robust datasets for monitoring land surface thermal dynamics (Li et al., 2023). Therefore, this study employs the version 6.1 MODIS monthly LST products, namely MOD11C3 (Terra) and MYD11C3 (Aqua), which provide global monthly mean LSTs at nominal observation times of 10:30/22:30 local solar time for Terra and 13:30/01:30 for Aqua, respectively, with a spatial resolution of 0.05 °. Both datasets are generated using the standard day/night algorithm (Wan and Li 1997) and further filled with data derived from the generalized split window algorithm (Wan and Dozier 1996) to enhance spatial completeness. Within the FuSVeT framework, these two products serve as the primary thermal inputs, providing four representative instantaneous observations per month. These observations are used to construct the monthly mean diurnal cycle (MDC) model, which forms the basis for separating soil and vegetation component temperatures.

To support the global generation of GloSVeT, the skin temperature variable from the ERA5-Land reanalysis dataset was employed to simplify model parameters and constrain the retrieval of soil and vegetation component temperatures. The ERA5-Land product provides physically consistent and spatially continuous estimates of the surface thermal state, derived through data assimilation and land surface modeling (Muñoz-Sabater et al., 2021). It offers hourly skin temperature fields

https://doi.org/10.5194/essd-2025-682
Preprint. Discussion started: 9 March 2026

aggregated into monthly averages at a spatial resolution of 0.10 °, with long-term continuity from 1950 to the present, ensuring complete temporal coverage and global consistency. In this study, the ERA5-Land skin temperature data were resampled to 0.05 °using the nearest neighbour method to maintain spatial consistency with the MODIS LST inputs.

Fractional Vegetation Cover (FVC) was used to characterize the sub-pixel composition of soil and vegetation components, which is essential for temperature decomposition. The Global Land Surface Satellite (GLASS) FVC product is derived from MODIS surface reflectance data using high spatial resolution reference FVC and the general regression neural network approach (Jia et al., 2015). This product has been extensively validated and demonstrates accuracy comparable to other global FVC datasets, while offering superior spatial and temporal continuity. In this study, the 8-day 0.05 ° GLASS FVC product was employed and aggregated to monthly means to represent pixel-level vegetation structure, ensuring spatiotemporal consistency with the MODIS LST inputs and facilitating the global generation of GloSVeT.

Since the ERA5-Land product provides seamless global coverage without explicit distinction between land and non-land surfaces, additional land cover information was required to exclude non-vegetated areas such as water bodies and permanent snow or ice (Liu et al., 2025). To ensure consistency with the MODIS-based inputs, this study employed the version 6.1 MODIS Land Cover Type Yearly Global 0.05 °product (MCD12C1), which provides annual global land cover classification derived from MODIS surface reflectance data using the International Geosphere Biosphere Programme (IGBP) scheme (Sulla-Menashe et al., 2019). In this study, pixels identified as water bodies (IGBP type = 17) or permanent snow/ice (IGBP type = 15) were excluded based on the MCD12C1 land cover map, ensuring that GloSVeT represents only vegetated and baresoil surfaces.

2.2 Data used for GloSVeT evaluation

To evaluate the accuracy, consistency, and physical reliability of the GloSVeT dataset, multiple independent data sources were employed, including ground-based observations, reanalysis products, and environmental indicators (Table 2). These datasets support three complementary validation strategies: site-based comparison, TC analysis, and indicator-based consistency assessment.

https://doi.org/10.5194/essd-2025-682
Preprint. Discussion started: 9 March 2026

Variable	Dataset	Spatial Resolution	Temporal Resolution	Period	Purpose
Longwave radiation	Five flux observation networks (He et al., 2025)	Point (~40–80m footprint)	Instantaneous	2003-2023	Site-based validation using flux tower radiation data
Normalized difference vegetation index	Landsat Collection 2 Tier 1 NDVI composite	30m	8-day	2003-2023	Determination of flux site surface type (soil, vegetation, or mixed)
Top-layer soil temperature	ERA5-Land/ GLDAS	0.10 ° 0.25 °	Monthly	2003-2023	TC analysis for soil temperature
Air temperature	ERA5-Land/ GLDAS	0.10 ° 0.25 °	Monthly	2003-2023	TC analysis for vegetation temperature
Soil moisture	ESA CCI SM	0.25 °	Daily	2003-2023	Indicator-based assessment of soil temperature consistency
Solar-induced fluorescence	GOSIF	0.05 °	8-day	2003-2023	Indicator-based assessment of vegetation temperature consistency

Table 2. Data used for the evaluation of the GloSVeT product

The temperature-based validation approach is the most straightforward means of assessing the accuracy of temperature products, as it directly compares satellite-retrieved temperatures with concurrent ground-based measurements (Li et al., 2023). Using random forest modelling and Landsat LST data, He et al., (2025) systematically evaluated the spatial representativeness of 211 flux sites from five observation networks worldwide. Following their findings, this study selected 46, 36, 49, and 62 sites exhibiting strong spatial representativeness across multiple scales (1 km, 3 km, 5 km, and 10 km) for spring, summer, autumn, and winter, respectively. For these sites, available upwelling and downwelling longwave radiation data from 2003 to 2023 were collected to calculate site-level instantaneous LST using the following equation (Xing et al., 2021).

$$T_i = \left[\frac{L_u - (1-\varepsilon_b) \times L_d}{\sigma \times \varepsilon_b} \right] \quad (1)$$

where T_i is the instantaneous temperature; L_u and L_d are the upwelling and downwelling longwave radiation, respectively; σ is the Stefan–Boltzmann constant (5.670373 $\times 10^{-8}$ W/m^2/K^4); and ε_b is the broadband emissivity, calculated using spectral emissivities from the Cooperative Institute for Meteorological Satellite Studies (CIMSS) baseline-fit emissivity database (http://cimss.ssec.wisc.edu/iremis/) as input, following a linear conversion method (Cheng et al., 2013). Subsequently, all instantaneous LST estimates, regardless of clear-sky or cloudy conditions, were averaged to derive the true monthly mean LST (Xing et al., 2021). The effective observational footprints of these flux towers typically range from 40 to 80 m in diameter. To determine whether the measured LST corresponds to soil, vegetation, or a mixed surface, we additionally used the Landsat Collection 2 Tier 1 Level-2 8-day 30m normalized difference vegetation index (NDVI) composite (https://developers.google.com/earth-engine/datasets/catalog/LANDSAT_COMPOSITES_C02_T1_L2_8DAY_NDWI).

https://doi.org/10.5194/essd-2025-682
Preprint. Discussion started: 9 March 2026

Specifically, the 8-day NDVI values at each site were aggregated to monthly means, and the thermal measurements were classified as soil, vegetation, or mixed when the corresponding NDVI was ≤ 0.1, ≥ 0.7, or in between, respectively.

Two reanalysis datasets, ERA5-Land (Muñoz-Sabater et al., 2021) and GLDAS (Rodell et al., 2004), were used to perform the TC analysis. The ERA5-Land product provides monthly averaged variables at a spatial resolution of 0.10°, while GLDAS offers 0.25° resolution. To ensure comparability, only the top-layer soil temperature was used from both datasets. Specifically, the monthly mean soil temperature level 1 from ERA5-Land and the SoilTMP0_10cm_inst variable from GLDAS were employed. For vegetation temperature, the air temperature was used as a proxy in densely vegetated regions, given the strong coupling between canopy and near-surface air temperature (Li et al., 2001; Rutter et al., 2023; Zhan et al., 2011). Correspondingly, the monthly mean 2m temperature from ERA5-Land and Tair_f_inst from GLDAS were used. For the TC analysis, both the GloSVeT soil and vegetation temperatures and the ERA5-Land soil and air temperatures were aggregated to a 0.25° spatial resolution to match the GLDAS grid. In addition, the GLASS FVC product was aggregated to 0.25° to identify densely vegetated pixels (FVC ≥ 0.8) for vegetation temperature evaluation.

To evaluate the physical consistency of GloSVeT, we examined the relationships between soil temperature and soil moisture, as well as between vegetation temperature and SIF. These analyses were designed to assess whether the spatial and temporal variations in GloSVeT are consistent with the expected energy–water–carbon interactions derived from theory and independent observations. For this purpose, we used the European Space Agency Climate Change Initiative Soil Moisture (ESA CCI SM) product, which provides a long-term, quality-controlled global record (1978–present) generated through a multi-sensor merging algorithm (Dorigo et al., 2017; Gruber et al., 2019). The dataset offers daily global coverage at 0.25° spatial resolution. In this study, the SM data were averaged to monthly means, and the GloSVeT soil temperatures were aggregated to 0.25° to ensure spatial comparability. For vegetation, we used the GOSIF dataset, a global SIF product derived from discrete OCO-2 soundings, MODIS observations, and meteorological reanalysis inputs using a data-driven approach (Li and Xiao 2019). GOSIF provides 8-day SIF estimates at 0.05° resolution for the period 2000–2024 and shows strong agreement with GPP from 91 FLUXNET sites, i.e., the coefficient of determination (R^2) = 0.73 and $p < 0.001$. In this study, the SIF data were aggregated to monthly means to match the temporal scale of GloSVeT and used to examine the correspondence between vegetation temperature and photosynthetic activity.

3 Method

3.1 FuSVeT

In the FuSVeT framework, the temporal variations of soil and vegetation temperatures at the monthly scale are described using an MDC model. In this study, the well-established GOT09 model (Göttsche and Olesen 2009) was adopted to represent sub-daily temperature dynamics, as expressed in Eq.s (2)–(6).

https://doi.org/10.5194/essd-2025-682
Preprint. Discussion started: 9 March 2026

$$\begin{cases} T_{day}(t) = T_0 + T_a \cos(\theta_z)\cos^{-1}(\theta_{z,\min}) \cdot e^{\left[m_{\min} - m(\theta_z)\right]\tau}, t < t_s \\ T_{night}(t) = T_0 + \delta T + \left[T_a \cos(\theta_{zs})\cos^{-1}(\theta_{z,\min}) \cdot e^{\left[m_{\min} - m(\theta_{zs})\right]\tau} - \delta T\right] e^{\frac{-12}{\pi k}(\theta - \theta_s)}, t \geq t_s \end{cases} \quad (2)$$

$$\theta = \frac{\pi}{12}(t - t_m) \quad (3)$$

$$\theta_z = \arccos\left(\sin(\delta)\sin(\phi) + \cos(\delta)\cos(\phi)\cos(\theta)\right) \quad (4)$$

$$m(\theta_z) = -\frac{R_E}{H}\cos(\theta_z) + \sqrt{\left[\frac{R_E}{H}\cos(\theta_z)\right]^2 + 2\frac{R_E}{H} + 1} \quad (5)$$

$$k = \frac{12}{\pi}\frac{\cos(\theta_{zs}) - \frac{\delta T}{T_a}\frac{\cos(\theta_{z,\min})}{e^{(m_{\min} - m(\theta_{zs}))\tau}}}{\frac{d\theta_z(\theta_s)}{d\theta}\sin(\theta_{zs}) + \tau\cos(\theta_{zs})\frac{\partial m(\theta_{zs})}{\partial \theta_z}} \quad (6)$$

where $T_{day}(t)$ and $T_{night}(t)$ denote the day and night temperature variations at time t, respectively; T_0 is the temperature around sunrise; T_a is the diurnal temperature amplitude; t_m is the time of maximum temperature; t_s is the time marking the onset of free attenuation, representing the transition between daytime heating and nighttime cooling; τ is the atmospheric transmittance; δT is the day-to-day change of residual temperature; θ is the thermal hour angle; θ_z is the solar zenith angle; $\theta_{z,min}$ is the minimum solar zenith angle and can be calculated using Equation (4) at θ=0; m is the relative air mass; m_{min} is the minimum relative air mass, and can be obtained using Equation (5) at θ_z=$\theta_{z,min}$; θ_s is the thermal hour angle for t=ts; θ_{zs} is the thermal zenith angle derived from Equation (4) at θ=θs; R_E is the radius of the Earth, and H is the scale height of the atmosphere. This model contains six free parameters: T_0, T_a, t_m, t_s, δT, and τ.

Based on geometrical theory and the MDC model, the relationship between LST and two component temperatures can be expressed as:

$$T(t) = \left[\frac{fvc \cdot \varepsilon_v \cdot \left[MDC(T_{0,v}, T_{a,v}, t_{m,v}, t_{s,v}, \delta T_v, \tau)\right]^4 + (1 - fvc) \cdot \varepsilon_s \cdot \left[MDC(T_{0,s}, T_{a,s}, t_{m,s}, t_{s,s}, \delta T_s, \tau)\right]^4}{fvc \cdot \varepsilon_v + (1 - fvc) \cdot \varepsilon_s}\right]^{0.25} \quad (7)$$

where T is the LST for a mixed pixel; the subscripts s and v represent the MDC parameters for soil temperature and vegetation temperature, respectively; ε_v and ε_s are the broadband emissivities for vegetation component and soil component, set to 0.98 and 0.95 in this study; fvc is the fractional vegetation cover. Accordingly, the retrieval of soil and vegetation temperatures becomes equivalent to solving for the eleven MDC parameters, i.e., $T_{0,s}$, $T_{a,s}$, $t_{m,s}$, $t_{s,s}$, δT_s, $T_{0,v}$, $T_{a,v}$, $t_{m,v}$, $t_{s,v}$, δT_v, and τ.

The core principle of FuSVeT is to partition all MDC parameters into temperature-independent and temperature-dependent groups, and solve them through a multi-source data fusion strategy to ensure physical consistency and spatial completeness.

https://doi.org/10.5194/essd-2025-682
Preprint. Discussion started: 9 March 2026

Specifically, temporally dense reanalysis data are used both to directly estimate the temperature-independent parameters and to provide initial values and physical constraints for the temperature-dependent parameters. The temperature-dependent parameters are subsequently optimized using temporally sparse satellite observations. Further methodological details can be found in Liu et al., (2025).

3.2 Generation of GloSVeT using the FuSVeT method

The overall technical workflow for generating the GloSVeT dataset is illustrated in Figure 1. The process begins with parameter initialization using ERA5-Land skin temperature and the spatially and temporally upscaled monthly GLASS FVC data at 0.10 ° spatial resolution. These datasets are jointly employed to estimate seven temperature-independent and four temperature-dependent parameters within the original MDC model. To ensure physical realism, a temperature difference constraint between soil and vegetation components (−10 K to 30 K) was imposed, and parameter optimization was carried out using a Bayesian optimization algorithm (Pelikan 2005). The retrieved parameters were subsequently downscaled to 0.05 ° by uniformly assigning them to the corresponding 2 × 2 finer pixels. After parameter reduction, a simplified four-parameter MDC model was constructed. By combining the 0.05 ° GLASS FVC and MOD11C3/MYD11C3 LST products, the temperature-dependent parameters were further refined to establish a calibrated MDC model. Based on this model, 24 hourly temperature steps were simulated to derive instantaneous soil and vegetation temperatures, which were then averaged temporally to obtain the final monthly mean component temperatures.

https://doi.org/10.5194/essd-2025-682
Preprint. Discussion started: 9 March 2026

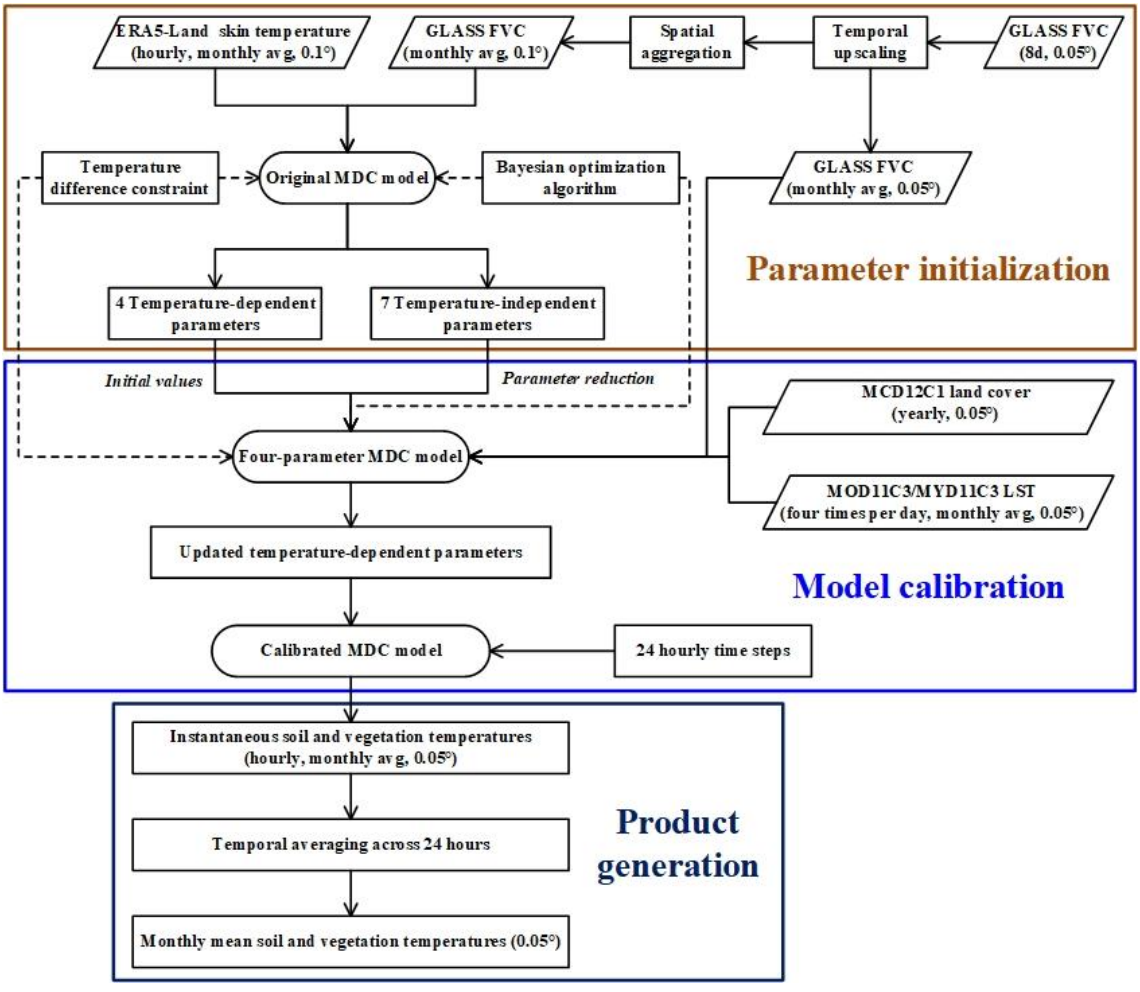

Figure 1: Workflow for generating the GloSVeT dataset using the FuSVeT method.

To enhance computational efficiency and retrieval accuracy, several technical refinements were implemented. First, the MCD12C1 land cover dataset was used to exclude non-vegetated pixels such as water bodies and permanent snow or ice, thereby reducing computational load and improving the robustness of the results. Second, since the Bayesian optimization algorithm requires numerous iterations to approximate the solution distribution, the computation can be highly time-consuming. Based on empirical tests, the iteration number was set to 2000 to achieve a balance between accuracy and efficiency. Finally, because errors in the MYD11C3 nighttime viewing time are known to introduce artificial patterns over the region of 20 ℃–30 ℃ (see Figs. 8a and 9a in Liu et al., 2025), a correction was applied: when nighttime values exceeded their theoretical range (00:00–03:00), they were replaced with the corresponding daytime values shifted by 12 hours.

https://doi.org/10.5194/essd-2025-682
Preprint. Discussion started: 9 March 2026

3.3 Evaluation and consistency analysis

The TC analysis was applied to quantify random uncertainties in soil and vegetation temperatures without relying on in situ measurements. This method assumes that three independent datasets describe the same geophysical variable through linear relationships, and that their random errors are mutually uncorrelated (Gruber et al., 2016; Park et al., 2023; Stoffelen 1998). By exploiting the covariance structure among the three datasets, the relative random errors and mutual consistency can be estimated in a statistically robust manner. In this study, TC was implemented to evaluate the reliability of GloSVeT against ERA5-Land and GLDAS for both soil and vegetation component temperatures. The analysis was conducted on a monthly basis from 2003 to 2023 using detrended monthly anomalies of each dataset to minimize large-scale systematic differences and emphasize temporal co-variability. The resulting correlation coefficients provide spatially explicit diagnostics of relative reliability and spatiotemporal stability, allowing identification of regions where the GloSVeT retrievals exhibit higher or lower agreement with independent datasets.

An anomaly–based correlation analysis was conducted to evaluate whether the temporal dynamics of GloSVeT are physically consistent with hydrological processes and photosynthetic activity. For the soil component, correlations between soil temperature anomalies and soil moisture anomalies were analyzed to assess their co-variation and potential phase lag across different biomes. Both positive and negative time lags (from −3 to +3 months) were considered to capture delayed or advanced soil thermal responses to moisture variability, providing insight into the coupling strength between surface energy and water processes. For the vegetation component, correlations between vegetation temperature anomalies and SIF anomalies were examined to determine whether temperature fluctuations correspond to variations in photosynthetic activity. The analysis was restricted to the growing season, defined as the period when the climatological mean SIF exceeded its 30th percentile within the annual cycle and persisted for at least two consecutive months. This restriction ensures that the temperature–SIF relationships reflect periods of active vegetation functioning.

4 Results and discussion

4.1 Site-based validation

The accuracy of GloSVeT soil and vegetation temperatures was evaluated against ground-based measurements from flux tower networks over the period 2003–2023 (Figure 2). For soil temperature (T_s), the R^2 ranged from 0.84 to 0.98, with biases between −1.0 K and −1.9 K and RMSE values of 1.6–2.2 K. For vegetation temperature (T_v), the performance was similarly robust, with R^2 values of 0.90–0.96, biases of −1.1 K to −1.9 K, and RMSE values of 1.7–3.0 K. Across all sites and seasons, GloSVeT exhibited a consistent underestimation of approximately 1–2 K for both components. This systematic offset may result from the uneven temporal distribution of satellite observations, leading to imperfect representation of near-sunrise temperature conditions within the monthly mean diurnal cycle model (Götsche and Olesen 2009; Liu et al., 2025).

https://doi.org/10.5194/essd-2025-682
Preprint. Discussion started: 9 March 2026

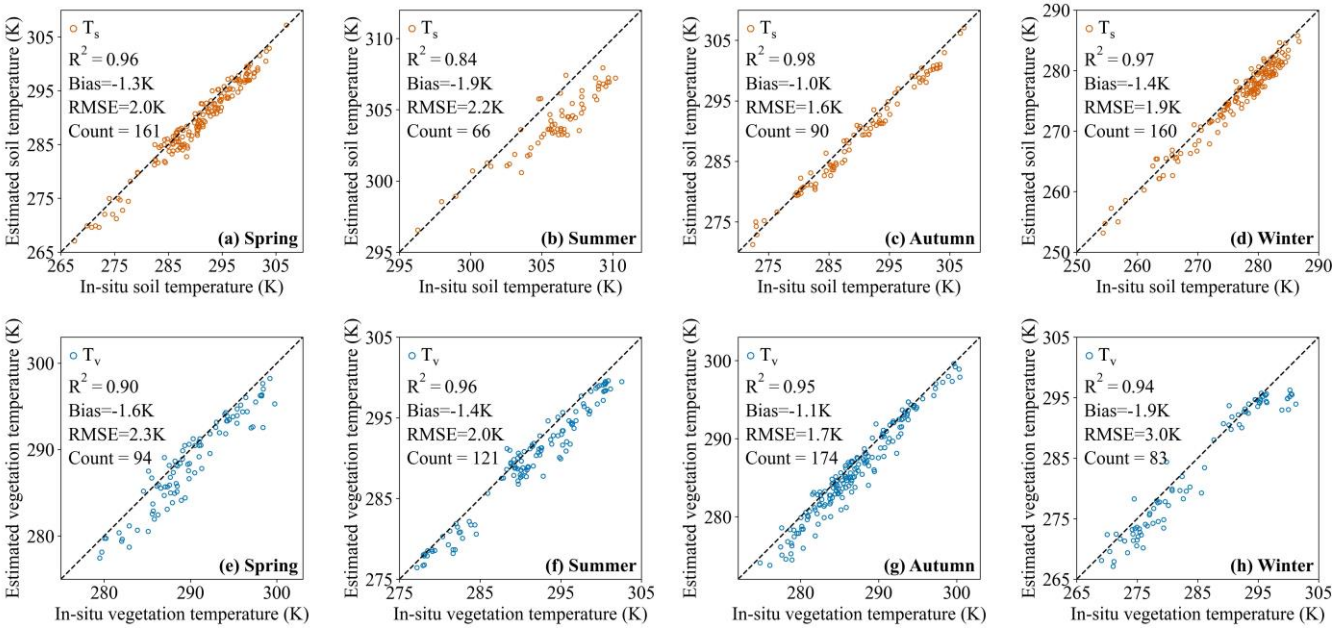

Figure 2: Validation of GloSVeT against in-situ measurements across different seasons. Panels (a–d) show soil temperature (T_s), and panels (e–h) show vegetation temperature (T_v). The dashed line represents the 1:1 reference line.

Seasonal variations in accuracy are evident. For soil temperature, performance was slightly lower in summer (R^2 = 0.84, RMSE = 2.2 K), likely due to the limited number of available sites (count = 66) and the strong influence of dense vegetation cover (Liu et al., 2020b; Zhan et al., 2011; Zhan et al., 2013). In contrast, vegetation temperature retrievals showed larger errors in winter (RMSE = 3.0 K), which may be attributed to fewer flux tower observations (count = 83) and sparse canopy conditions. The highest agreement occurred in autumn for both components, when vegetation and atmospheric conditions were relatively stable, resulting in minimal uncertainty during component separation.

Overall, these results confirm that GloSVeT achieves consistent and physically reasonable performance across seasons, with strong correlations (R^2 > 0.9 in most cases) and low RMSE values (typically < 2 K), effectively reproducing surface component temperatures at the monthly scale.

4.2 TC-based uncertainty evaluation

Figure 3 shows the results of the TC-based correlation (R) for soil temperature. In general, the three products exhibit largely consistent spatial patterns (Figure. 3a–c) and latitudinal variation (Figure. 3d). High correlations (R > 0.7) are found mainly in the Northern Hemisphere high latitudes and the humid tropics, whereas low correlations (R < 0.5) appear in many mid-latitude transitional regions. This spatial coherence across independent datasets indicates that the major large-scale thermal variations are consistently captured among the different data sources, and further supports the physical plausibility of the GloSVeT retrievals.

https://doi.org/10.5194/essd-2025-682
Preprint. Discussion started: 9 March 2026

Although their overall patterns are similar, some differences can be observed among the three datasets. ERA5-Land shows the highest correlations north of 30 °N but performs poorly elsewhere, particularly in tropical regions between 30 °S and 30 °N (Figure. 3d). Its distribution contains a larger share of both very high ($R > 0.8$) and very low ($R < 0.4$) correlations (Figure. 3e, f), reflecting spatial heterogeneity and limited stable behaviour. In contrast, GLDAS and GloSVeT achieve more equivalent performance (Figure. 3e, f). However, GLDAS has fewer strong-correlation pixels ($R > 0.8$), whereas GloSVeT exhibits a smoother and more concentrated distribution toward higher R values (Figure. 3e), implying spatially homogeneous and strong stability. Remarkably, GloSVeT performs best in tropical rainforest regions such as the Amazon and the Congo Basin, underscoring its advantage in these environmentally sensitive and data-scarce areas. By contrast, its correlations are slightly lower at high latitudes. This may occur because ERA5-Land and GLDAS represent layer-averaged subsurface soil temperatures, whereas GloSVeT retrieves surface soil temperature which is more sensitive to snow cover and radiation inversions (Cao et al., 2023; Liu et al., 2025). Taken together, the TC-based evaluation suggests that while reanalyses perform better in high-latitude regions, GloSVeT achieves a more balanced and stable representation globally, with clear strengths in humid tropical regions, thereby providing a reliable soil temperature component for large-scale applications.

https://doi.org/10.5194/essd-2025-682
Preprint. Discussion started: 9 March 2026

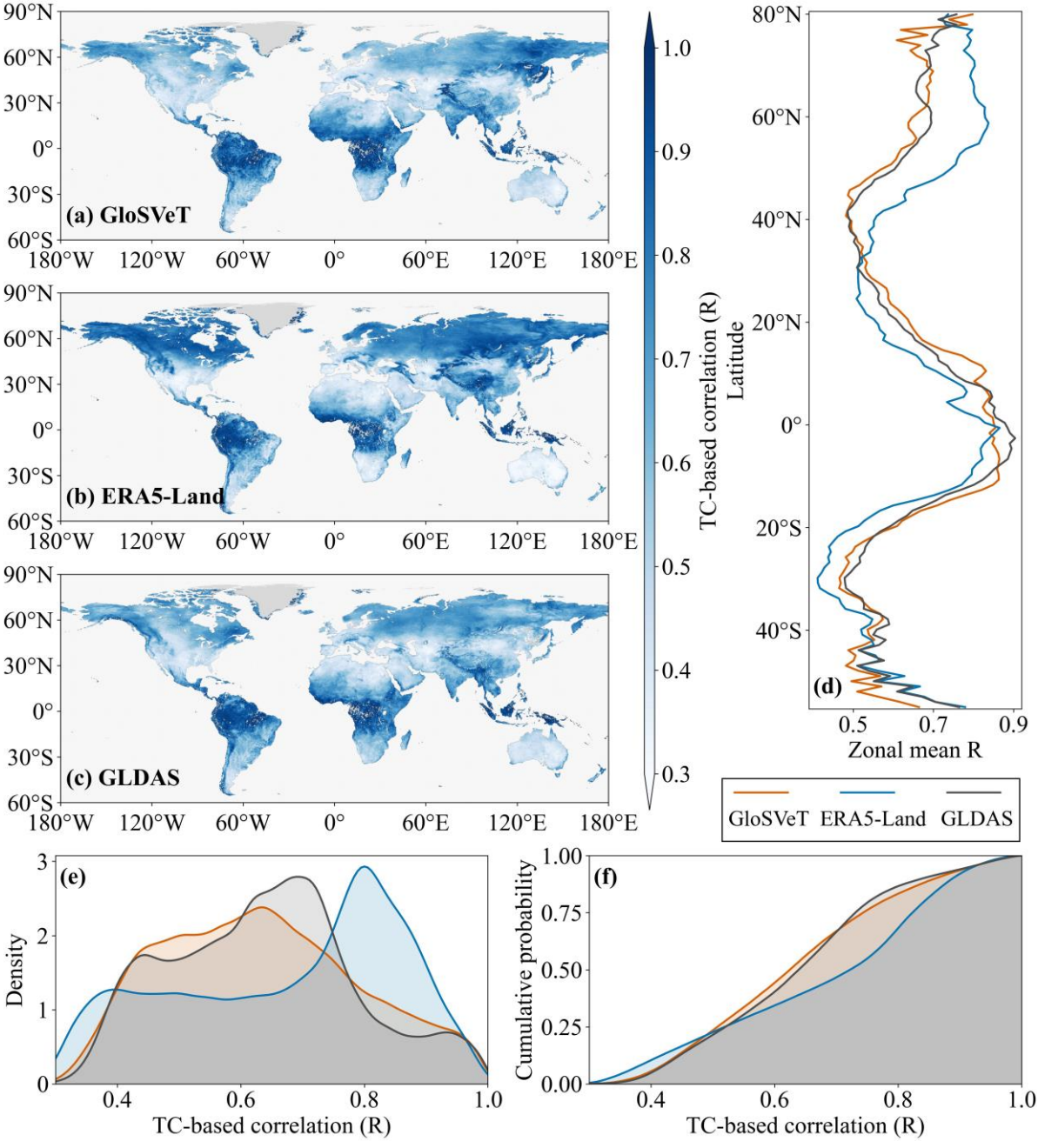

Figure 3: TC-based correlation (R) for soil temperature. Panels (a–c) illustrate the spatial distributions for GloSVeT, ERA5-Land, and GLDAS, respectively, with light gray and medium gray indicating the ocean and land backgrounds; (d) shows the zonal-mean R as a function of latitude; and panels (e) and (f) present the probability density and cumulative distribution functions, respectively.

To extend the assessment from a global view to ecosystem contexts, this study further compared TC-based correlations for soil temperature across 14 biome types (Figure 4). In general, the three datasets show higher median correlations (R ≈ 0.7–

https://doi.org/10.5194/essd-2025-682
Preprint. Discussion started: 9 March 2026

0.9) in cold high-latitude and humid tropical ecosystems, such as temperate coniferous and mixed forests, boreal forests, tundra (Figure 4e, 4f, 4k), and tropical moist broadleaf forests and mangroves (Figure 4a, 4n). In contrast, lower correlations (R ≈ 0.5) with larger spreads are observed in Mediterranean, arid, and temperate grassland systems (Figure 4l, 4m, 4h). This cross-biome consistency reinforces that large-scale soil thermal variations are physically coherent across independent datasets and that the GloSVeT retrievals remain robust under diverse hydrothermal regimes.

Among the three products, GLDAS and GloSVeT exhibit comparable performance across most biomes, whereas ERA5-Land shows the largest inter-biome variability. ERA5-Land performs best in cold and mid-latitude forest ecosystems, such as boreal forests, tundra, montane grasslands, and temperate mixed or coniferous forests (Figure 4f, 4k, 4j, 4d, 4e), but its correlations drop markedly in tropical and semi-arid regions. Its boxplots also display wider interquartile ranges, indicating higher spatial heterogeneity and weaker internal consistency. By contrast, GloSVeT maintains more consistent correlations across biomes, with notably stronger performance in tropical dry broadleaf forests, tropical/subtropical grasslands, savannas and shrublands, flooded grasslands, and deserts/xeric shrublands (Figure 4b, 4g, 4i, 4m). Overall, these biome-specific results align with the global patterns in Figure 3, reinforcing the robustness of GloSVeT and its evident advantages in humid tropical and moisture-variable environments.

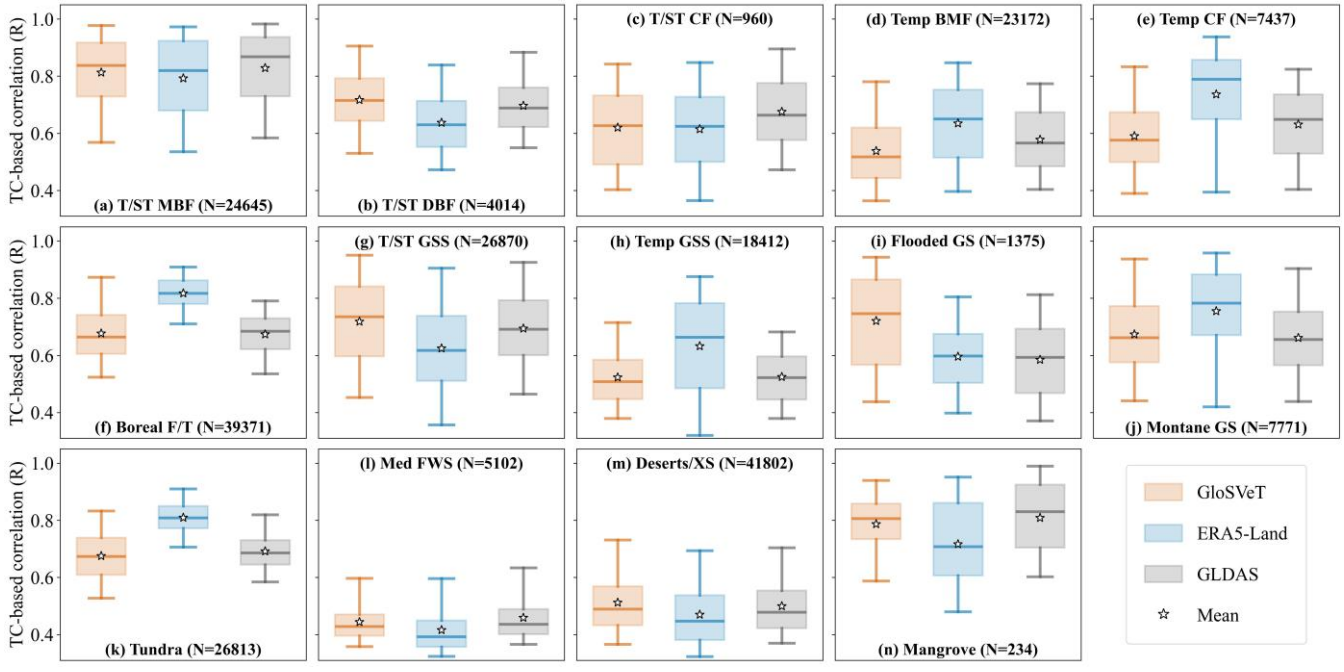

Figure 4: TC-based correlation (R) for soil temperature across 14 major biomes. Boxplots show the distributions of R for GloSVeT (vermillion), ERA5-Land (blue), and GLDAS (dark gray). Stars denote the mean values. T/ST, MBF, DBF, CF, Temp, BMF, F/T, GSS, GS, Med, FWS, and XS, are the abbreviations of Tropical/subtropical', 'moist broadleaf forests', 'dry broadleaf forests', 'coniferous forests', 'Temperate', 'broadleaf and mixed forests', 'forests/taiga', 'grasslands, savannas and shrublands', 'grasslands and savannas', 'Mediterranean', 'forests, woodlands and scrub or sclerophyll forests', and 'xeric shrublands', respectively.

https://doi.org/10.5194/essd-2025-682
Preprint. Discussion started: 9 March 2026

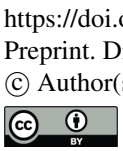

Figure 5 and Figure 6 present the TC-based correlations for vegetation temperature. Since the analysis was restricted to densely vegetated pixels, and only pixels with more than 100 matched pairs were included to ensure the reliability of TC estimation, resulting in coverage mainly over tropical and subtropical regions. Similar to the soil component, the three datasets display broadly consistent spatial and latitudinal patterns, yet GloSVeT systematically exhibits higher correlations and a narrower spread. As shown in Figures 5a–d, across South America, Africa, and Southeast Asia, GloSVeT achieves stronger and more spatially uniform correlations (R > 0.8) than ERA5-Land and GLDAS. The probability density and cumulative distribution curves (Figures 5e,f) further indicate that GloSVeT contains a greater fraction of high R pixels and fewer low R outliers, reflecting improved temporal coherence and spatial stability. When compared across major vegetation types (Figure 6), GloSVeT maintains the highest or comparable median correlations in tropical moist and dry broadleaf forests, temperate mixed forests, and tropical/subtropical grasslands, underscoring its superior performance in representing canopy thermal dynamics across diverse hydroclimatic conditions.

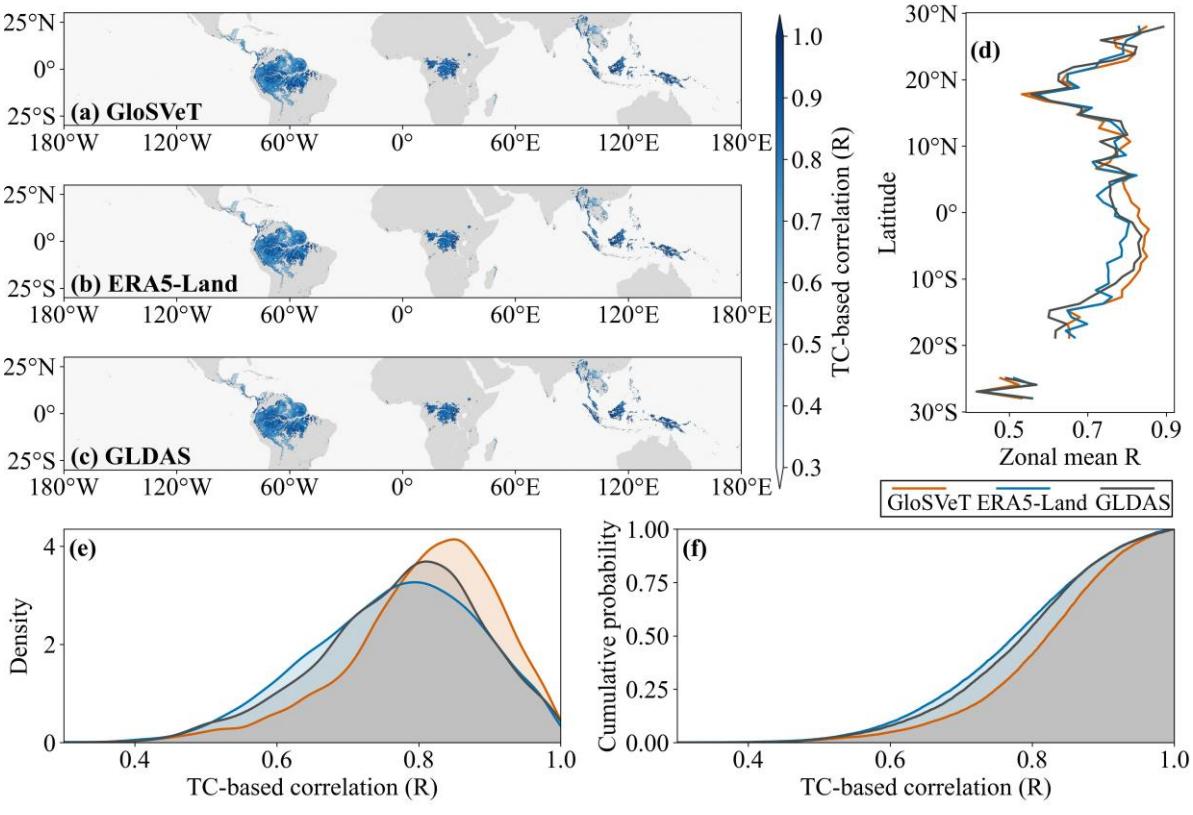

Figure 5: Same as Figure 3 but for vegetation temperature.

https://doi.org/10.5194/essd-2025-682
Preprint. Discussion started: 9 March 2026

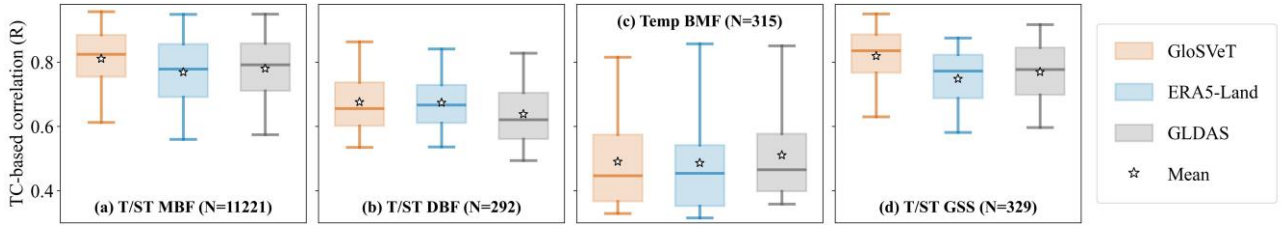

Figure 6: Same as Figure 4 but for vegetation temperature.

4.3 Physical consistency validation

Figure 7 illustrates the correlation between GloSVeT soil temperature anomalies and ESA CCI soil moisture anomalies under different lag conditions. At the global scale (Figure 7a), most (77.6%) significant pixels exhibit negative correlations (blue shading), indicating that wetter soil conditions are generally associated with lower soil temperatures. This spatially pervasive inverse relationship reflects the fundamental energy partitioning mechanism, where increased soil moisture enhances latent heat flux at the expense of sensible heating, leading to surface cooling. This mechanism has been well documented in both modeling and satellite-based studies (Benson and Dirmeyer 2021; Gurung and Chen 2024; Seneviratne et al., 2010). In contrast, positive correlations (22.4%; red shading) occur locally in high-latitude, arid, and coastal regions. These exceptions are mainly driven by processes such as snowmelt and freeze–thaw transitions at high latitudes (Hu et al., 2006; Jiang et al., 2023), precipitation pulses or irrigation in arid zones (Kong and Huber 2023; Manzoni et al., 2020), and coupled water–energy dynamics in coastal environments (Yu et al., 2024), all of which can produce synchronous increases in soil temperature and moisture.

Across biome types (Figures 7b–o), the proportion of significant pixels and the strength of soil temperature–moisture correlations exhibit distinct ecological patterns. Overall, the fraction of significant correlations is highest in montane grasslands (71.3%) and tropical/subtropical coniferous forests (69.5%), followed by Mediterranean woodlands (67.4%), tropical dry broadleaf forests (64.1%), and tropical/subtropical grasslands and savannas (60.1%). Intermediate proportions (≈50–55%) are observed in temperate grasslands and flooded grasslands, whereas high-latitude biomes such as boreal forests (38.0%) and tundra (31.7%) show much lower ratios. Mangroves have the lowest value (18.8%), likely due to their limited spatial extent and the strong influence of coastal hydrodynamics. This spatial gradient suggests that in topographically complex or hydrothermally contrasting mid- and low-latitude systems, soil moisture exerts a more coherent and consistent control on soil temperature (Seneviratne et al., 2010; Williams et al., 2009), while in cold regions the coupling is weakened by snow, permafrost, and heterogeneous freeze–thaw processes (Zhao et al., 2022).

Regarding correlation strength and lag dependence, most mid- and low-latitude biomes (e.g., montane grasslands, tropical forests, Mediterranean shrublands, and arid ecosystems) are dominated by zero-lag responses, with typically 40–60% of the significant pixels. This phenomenon indicates an immediate and direct soil moisture–temperature coupling through contemporaneous energy partitioning. Their median correlations are moderately negative (about −0.1 to −0.3) with relatively compact spreads, reflecting a stable hydrothermal interaction. In semi-arid and Mediterranean regions, however, preceding

https://doi.org/10.5194/essd-2025-682
Preprint. Discussion started: 9 March 2026


Open Access Earth System Science Data Discussions

(−1 to −2 month) effects are also evident, implying a leading influence of precipitation pulses or subsurface water recharge (Manzoni et al., 2020). In contrast, high-latitude biomes such as boreal forests and tundra show weaker and more variable correlations with increasing fractions of positive lags (+1 to +2 months), consistent with delayed soil thermal responses to snow accumulation and thawing (Cao et al., 2023). Flooded grasslands and coastal ecosystems display more scattered distributions and higher shares of negative lags, reflecting upstream inflows or periodic inundation that modulate both soil temperature and moisture simultaneously (Yu et al., 2024). Collectively, these biome-specific patterns suggest that GloSVeT effectively captures the spatially heterogeneous soil moisture–temperature coupling, ranging from the rapid, synchronous feedbacks of warm-humid regions to the lagged, inertia-dominated responses of high-latitude and hydrologically buffered systems. These results further demonstrate the capability of GloSVeT to robustly represent soil hydrothermal interactions across diverse climatic regimes.

https://doi.org/10.5194/essd-2025-682
Preprint. Discussion started: 9 March 2026

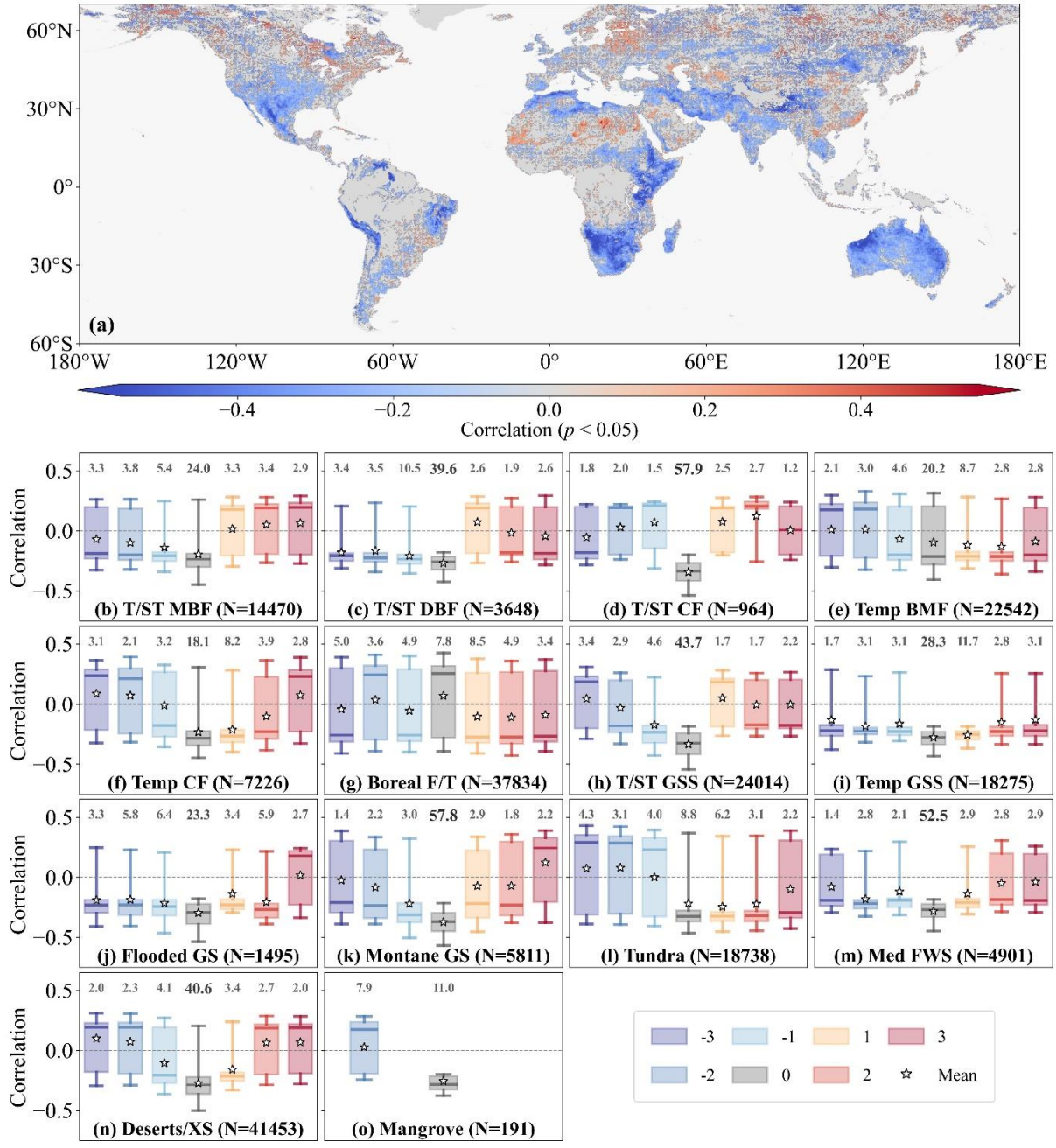

Figure 7: Correlation between GloSVeT soil temperature anomalies and ESA CCI soil moisture anomalies under different lag conditions. Panel (a) shows the spatial distribution of significant correlations (p < 0.05), where red and blue indicate positive and negative relationships, respectively. Panels (b–o) present the distribution of significant correlations across 14 major biomes. 395 **Boxplots with different colors denote different lag months (from −3 to +3). The numbers above each box indicate the percentage of significant pixels within the corresponding biome, with darker colors and larger font sizes representing higher proportions. N denotes the total number of pixels in each biome category.**

https://doi.org/10.5194/essd-2025-682
Preprint. Discussion started: 9 March 2026

At the growing-season scale, the relationship between GloSVeT vegetation temperature and SIF (Figure 8) exhibits clear large-scale regularities. As shown in Figure 8a, significant negative correlations dominate much of the subtropics and monsoon margins where soil moisture fluctuates strongly, indicating that warmer-than-normal canopies coincide with reduced photosynthetic activity. In contrast, positive correlations emerge mainly in energy-limited high-latitude regions, where moderate warming alleviates radiative or aerodynamic constraints and enhances photosynthetic efficiency. These contrasting patterns align well with the classical framework of water- versus energy-limited canopy functioning (Alkama and Cescatti 2016).

Regarding different biome types (Figure 8b), the correlation strength follows a distinct gradient from energy-limited to water-limited regimes. Boreal and temperate coniferous forests show the strongest positive correlations (~0.3) with compact distributions and high fractions of significant pixels (79.4% and 61.0%), indicating that canopy warming stimulates photosynthesis where energy supply constrains assimilation (Pan et al., 2024). Tundra exhibits similarly positive but less consistent correlations (34.1%), as snow and permafrost dampen the thermal–photosynthetic response. Transitional systems such as montane grasslands, temperate grasslands, and Mangrove around near-zero medians (absolute value < 0.2) with broad variability and limited significance (< 30%), reflecting mixed radiation–moisture control. The strongest negative couplings occur in flooded grasslands, tropical/subtropical dry broadleaf forests, tropical/subtropical grasslands–savannas, and deserts/xeric shrublands (median ~ −0.3 to −0.4), where canopy warming accompanies photosynthetic down regulation driven by water stress and stomatal closure (Doughty et al., 2023). Among these, tropical/subtropical savannas and dry forests show the most coherent relationships, while flooded and arid systems exhibit more dispersed patterns due to hydrological and edaphic heterogeneity. Collectively, these findings demonstrate that GloSVeT reliably captures the climate-dependent continuum of canopy thermal–photosynthetic coupling.

https://doi.org/10.5194/essd-2025-682
Preprint. Discussion started: 9 March 2026

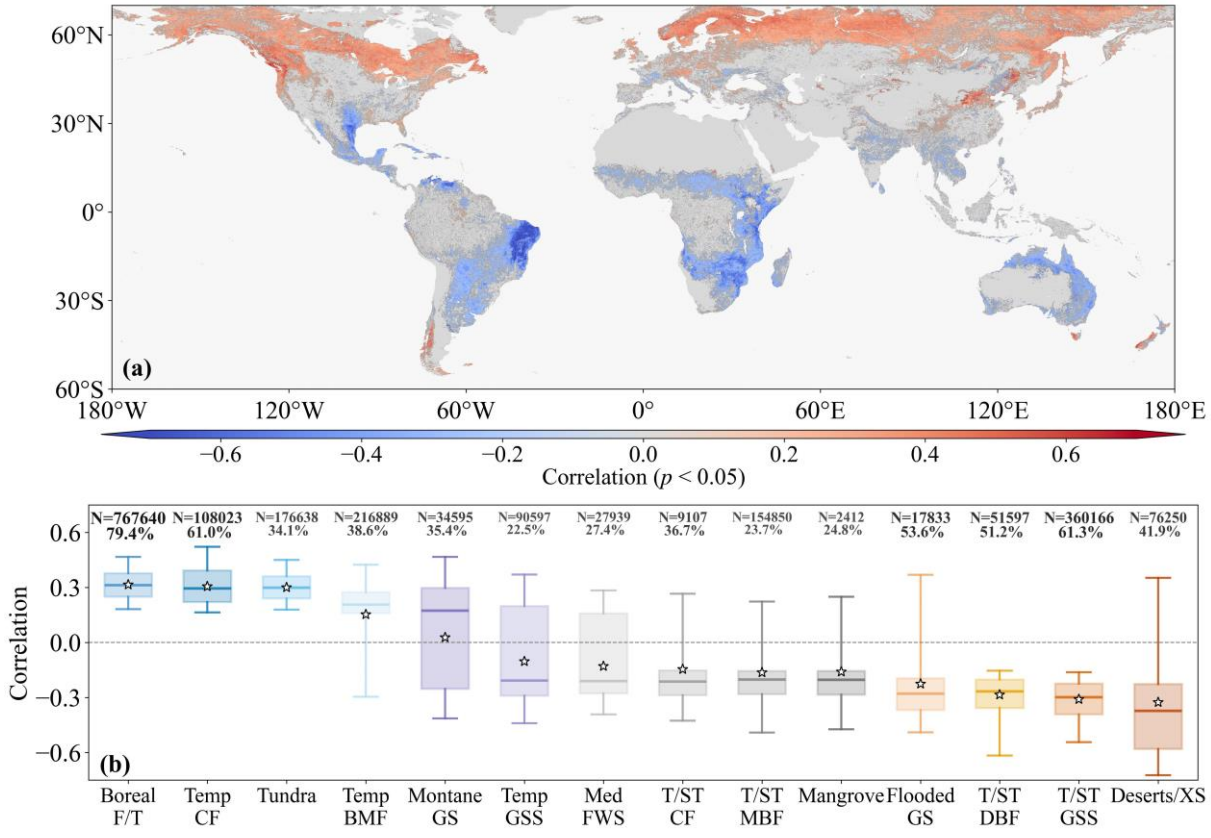

Figure 8: Correlation between GloSVeT vegetation temperature anomalies and GOSIF SIF anomalies. Panel (a) shows the spatial distribution of significant correlations (p < 0.05), where red and blue indicate positive and negative relationships, respectively. Panel (b) presents the distribution of significant correlations across 14 major biomes. The numbers above each box indicate the percentage of significant pixels within the corresponding biome, with darker colors and larger font sizes representing higher proportions. N denotes the total number of pixels in each biome category.

4.4 Spatiotemporal variability and trends

A unique advantage of the GloSVeT dataset is that it provides soil and vegetation temperatures simultaneously, enabling consistent evaluation of their co-variability and long-term evolution. Figure 9 illustrates the temporal trends of globally averaged component temperatures for the pixels where both soil temperature and vegetation temperature are available. These two time series exhibit highly synchronous variations across sub-seasonal to interannual scales, with peaks and troughs closely aligned, indicating that soil and vegetation temperature changes are dynamically coupled. In terms of long-term trends, both components show significant warming over 2003–2023, with slopes of 0.44 K/decade for soil temperature and 0.39 K/decade for vegetation temperature, suggesting slightly faster warming in the soil layer than in the canopy (Garcá-Garcá et al., 2023; Trew et al., 2024). The number of valid pixels ranges from 4.6×10^6 to 5.2×10^6, with a mean of 5.0×10^6 and a standard deviation of 0.1×10^6, confirming that the trend analysis is based on a stable and representative sample. The pixel count also exhibits a clear seasonal pattern, i.e., higher from June to October and lower in other months, which is

https://doi.org/10.5194/essd-2025-682
Preprint. Discussion started: 9 March 2026

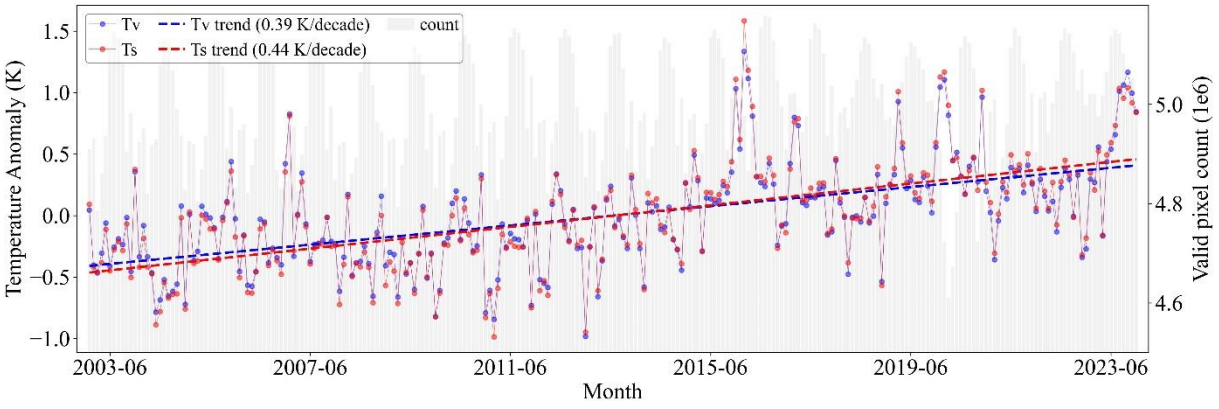

Figure 9: Global monthly anomalies of soil (T_s, red) and vegetation (T_v, blue) temperatures from 2003–2023. Dots show monthly means, dashed lines indicate linear trends, and grey bars (right axis) denote the number of valid pixels used each month.

To further investigate the spatial heterogeneity of these temporal trends, the linear slopes were mapped for representative cold (January) and warm (July) months (Figures 10–11). In January, the majority of pixels (68.4% for soil temperature and 62.3% for vegetation temperature) exhibit positive trends, indicating widespread wintertime warming. Pronounced warming occurs across North America, Europe, and southeastern China, whereas localized cooling is evident in northern Eurasia and the high Asian interior (Bartusek et al., 2022; Qiao et al., 2025). However, only a limited fraction of pixels reaches the 0.05 significance level (6.7% for soil temperature and 7.0% for vegetation temperature), mainly because the trend analysis for each calendar month is based on only 21 annual observations (2003–2023), which limits statistical power in regions with strong interannual variability. Even so, the significant trends are concentrated in the major warming and cooling centres, supporting the robustness of the large-scale spatial patterns. Compared with soil temperature, vegetation trends are generally weaker, consistent with the effects of snow masking, stronger canopy–air coupling during cold seasons, and the thermal buffering imposed by canopy structure and aerodynamic resistance (Forzieri et al., 2017). In the Southern Hemisphere, January trends are weaker and spatially patchier, reflecting the limited land area and weaker radiative forcing contrast during austral summer. In July, warming becomes more spatially extensive covering 74.8% of soil temperature and 70.7% of vegetation temperature pixels, but the overall rate is slightly lower. Broad warming is observed across the Northern Hemisphere mid-latitudes, particularly in western North America, the Mediterranean–Middle East, Central Asia, and northeastern China, whereas parts of Europe display moderate cooling. The proportion of statistically significant pixels increases in July (16.6% for soil temperature and 10.8% for vegetation temperature), indicating a stronger and more spatially coherent warm-season trend signal than in January. Consistent with the cold-season behaviour, soil temperature trends exceed those of vegetation temperature, reflecting the greater sensitivity of the soil skin to net radiation and the reduced evaporative buffering from vegetation (Qiao et al., 2023). In summary, these distinct seasonal behaviours, including stronger

https://doi.org/10.5194/essd-2025-682
Preprint. Discussion started: 9 March 2026

winter contrasts at high latitudes and widespread summer warming over continental interiors, confirm that GloSVeT realistically represents the global spatiotemporal structure of surface thermal change.

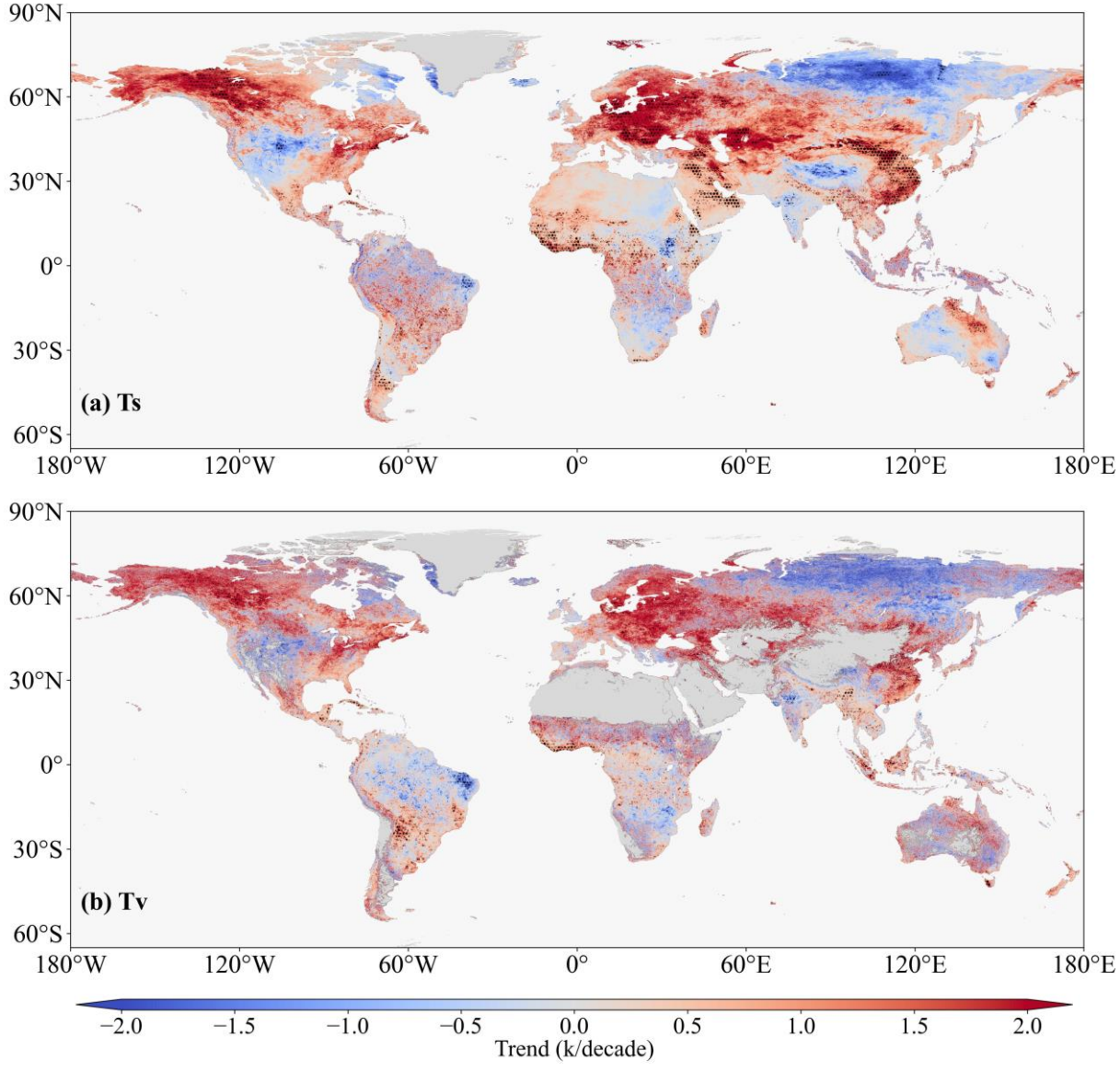

Figure 10: Linear trends of GloSVeT component temperatures in January for (a) soil and (b) vegetation during 2003–2023. Black dots indicate pixels with statistically significant trends ($p < 0.05$).

https://doi.org/10.5194/essd-2025-682
Preprint. Discussion started: 9 March 2026

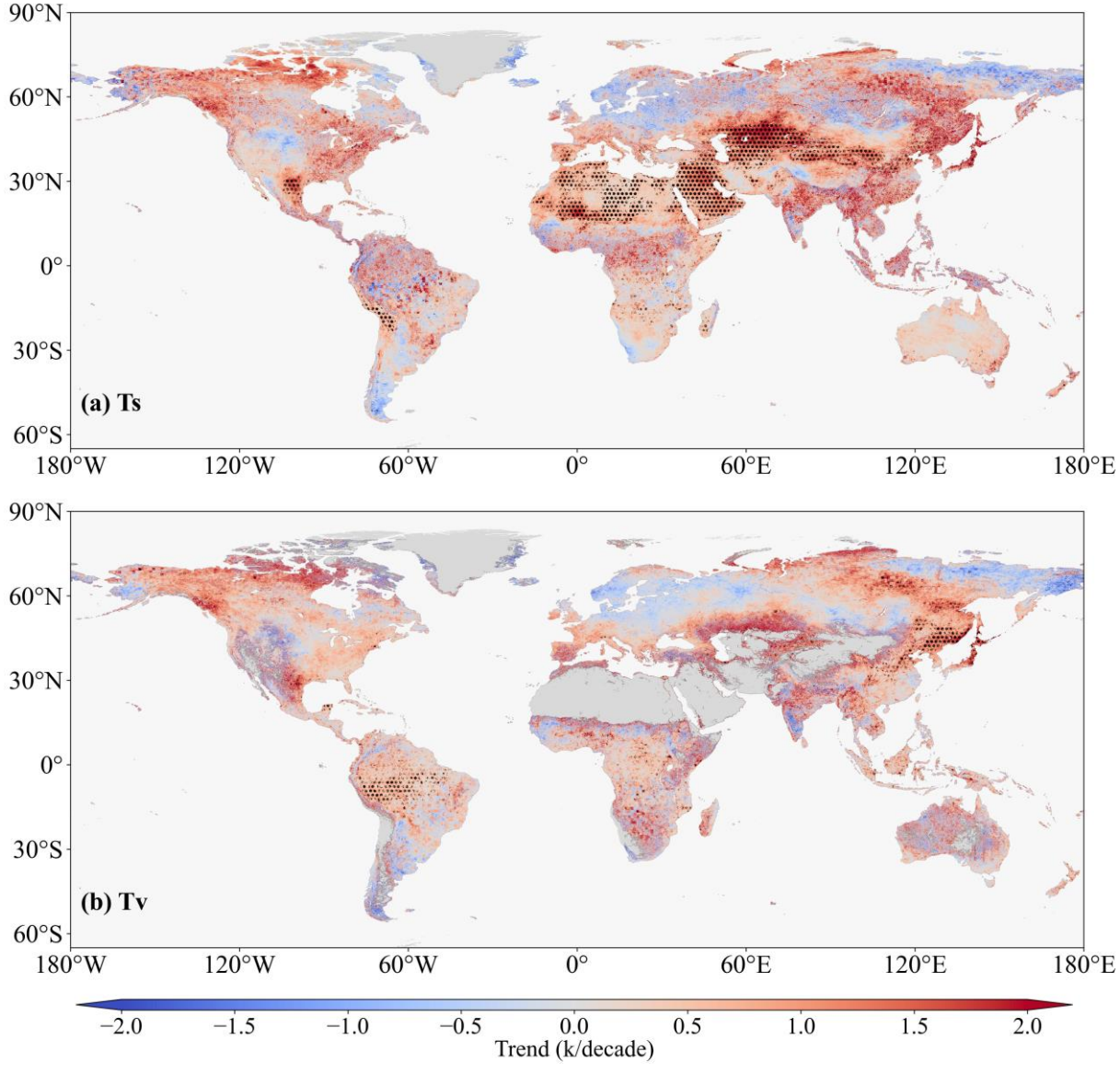

Figure 11: Same as Figure10 but in July.

4.5 Application potential and limitations

Based on extensive validation and consistency assessments, the GloSVeT dataset demonstrates high accuracy and strong physical consistency, offering broad potential for applications in land–atmosphere interaction studies, ecosystem monitoring, and model integration. First, by explicitly resolving the thermal contrast between soil and canopy, GloSVeT facilitates the separation of energy partitioning between soil evaporation and vegetation transpiration under varying vegetation covers. This capability is valuable for diagnosing surface–atmosphere coupling strength and improving the parameterization of energy

https://doi.org/10.5194/essd-2025-682
Preprint. Discussion started: 9 March 2026

balance models from regional to global scales (Li et al., 2023; Song et al., 2020). Second, the vegetation–soil temperature difference (ΔT) derived from GloSVeT is a physically based indicator that shows higher sensitivity to evaporative stress and canopy water deficit than the traditional canopy–air temperature difference (Luan and Vico 2021). By linking ΔT dynamics with soil moisture and vegetation optical indices, GloSVeT enables consistent detection of ecosystem drought responses and recovery trajectories across climatic gradients. Third, through the retrieval of spatially explicit and physically consistent vegetation temperatures, GloSVeT establishes key biophysical constraints for simulating crop productivity and terrestrial carbon exchange. Consequently, it can act as a robust alternative to conventional LST for coupling with photosynthetic metrics such as GPP to diagnose thermal stress impacts on crop performance and vegetation carbon assimilation (Prentice et al., 2024). Finally, owing to its global coverage, multi-decade record, and physically interpretable design, GloSVeT constitutes a valuable forcing or evaluation dataset for land surface and biogeochemical models. For instance, it can be incorporated into or benchmarked within modeling frameworks to improve the representation of surface thermal inertia, soil–canopy coupling, and energy–carbon feedbacks.

Despite its broad applicability, several limitations should be acknowledged. GloSVeT is currently produced at a monthly temporal resolution, reflecting a balance between computational efficiency and data availability. While this resolution is sufficient for climate-scale analyses, extending the dataset to daily scales would increase its value for near-real-time monitoring and process-level modeling (Li et al., 2022). In addition, the dataset currently reports only mean surface component temperatures, and the inclusion of additional thermal metrics based on temperature cycle models, such as diurnal range and maximum or minimum temperatures, would improve the representation of thermal variability and climate extremes (Li et al., 2023; Liu et al., 2023). Moreover, both the soil and vegetation temperatures in GloSVeT represent surface radiative states rather than subsurface or canopy internal conditions, which suggests that future versions could incorporate soil heat diffusion and canopy energy transfer schemes to better describe vertical thermal gradients (Cao et al., 2023; Lundquist et al., 2018). At the same time, although GloSVeT exhibits strong internal consistency and cross-site stability, uncertainties remain in regions affected by persistent cloud cover, snow, or complex terrain. Therefore, continued advances in data fusion, uncertainty quantification, and high-resolution retrieval techniques (Li et al., 2023; Zhao et al., 2025) will further enhance its accuracy and expand its relevance for Earth system science applications.

5 Code and data availability

The global 0.05 °monthly mean surface soil and vegetation component temperature dataset (GloSVeT) covering the period 2003–2023 is publicly available on https://doi.org/10.5281/zenodo.17461084 (Liu and Li, 2025) and https://data.tpdc.ac.cn/zh-hans/data/13b88dce-6bea-45f6-90e6-136e1fb57768 (Liu and Li, 2026). Data are provided as GeoTIFF files in UInt16 format with a scale factor of 0.02, expressed in Kelvin (K), and a fill value of 65535. The dataset can be directly accessed and used without any specialized software. The main code used for dataset generation, uncertainty

https://doi.org/10.5194/essd-2025-682
Preprint. Discussion started: 9 March 2026

evaluation, physical consistency validation, trend analysis, and figure reproduction is publicly available at GitHub: https://github.com/xyliu-TIR/GloSVeT.

6 Conclusions

Using the FuSVeT method adapted for global implementation, this study produced the first global dataset of soil and vegetation component temperatures (GloSVeT), providing monthly means at 0.05 ° spatial resolution for 2003–2023. To ensure reliability, a comprehensive multi-perspective evaluation was performed, integrating flux-tower validation, triple collocation analysis, physical consistency assessment, and spatiotemporal trend examination. Validation against flux-tower measurements demonstrated high accuracy for both components ($R^2 > 0.9$, RMSE ~ 2 K), with a minor, physically interpretable cool bias linked to the diurnal sampling of satellite observations. The triple collocation analysis further confirmed strong internal coherence and spatial robustness, showing globally consistent performance with distinct strengths in humid tropics and transitional environments, while reanalysis products performed relatively better at high latitudes. Physical consistency assessments revealed clear process-based relationships: soil temperature anomalies were negatively correlated with soil moisture, reflecting evaporative cooling, whereas vegetation temperature exhibited biome-dependent coupling with SIF, transitioning from positive correlations in energy-limited regions to negative ones in water-limited ecosystems. Spatiotemporal analyses showed significant warming trends in both soil (0.44 K/decade) and vegetation (0.39 K/decade) components during 2003–2023, with seasonally interpretable patterns characterized by stronger winter contrasts at high latitudes and widespread summer warming over continental interiors. Collectively, these results demonstrate that GloSVeT achieves physically consistent, spatially coherent, and dynamically realistic performance across diverse climatic regimes. Therefore, this new dataset is expected to provide a valuable foundation for quantifying land–atmosphere energy exchange, monitoring ecosystem hydrothermal dynamics, and improving the representation of surface processes in Earth system models.

Author contributions

XL and ZL developed the methodology and designed the experimental framework. XL processed the data and produced the dataset. CY assisted with data analysis and validation. ZL and SD provided guidance on method refinement and result interpretation. XL drafted the original manuscript, and all authors contributed to scientific discussions and manuscript revisions.

Competing interests

The contact author has declared that none of the authors has any competing interests.

https://doi.org/10.5194/essd-2025-682
Preprint. Discussion started: 9 March 2026

Acknowledgements

We would like to thank National Aeronautics and Space Administration for providing us the MOD11C3/MYD11C3, MCD12C1 and GLDAS data, European Centre for Medium-Range Weather Forecasts for providing ERA5-Land data, Global Land Surface Satellite for providing FVC data, United States Geological Survey for providing Landsat NDVI data, European Space Agency for providing SM data, Dr. Xing Li for providing GOSIF product, and six flux networks, i.e., AmeriFlux, SURFRAD, Euroflux, OzFlux, AsiaFlux, and ChinaFlux for providing in situ measurements.

Financial support

This research has been supported by the Central Public-interest Scientific Institution Basal Research Fund (No. Y2024QC17), and the National Natural Science Foundation of China (Grant No. 42101371, 41921001, and 42401442).

References

Alkama, R. and Cescatti, A.: Biophysical climate impacts of recent changes in global forest cover, Science, 351, 600-604, 10.1126/science.aac8083, 2016.

Bartusek, S., Kornhuber, K., and Ting, M.: 2021 North American heatwave amplified by climate change-driven nonlinear interactions, Nat. Clim. Change, 12, 1143-1150, 10.1038/s41558-022-01520-4, 2022.

Baumberger, M., Haas, B., Sivakumar, S., Ludwig, M., Meyer, N., and Meyer, H.: High-resolution soil temperature and soil moisture patterns in space, depth and time: An interpretable machine learning modelling approach, Geoderma, 451, 10.1016/j.geoderma.2024.117049, 2024.

Benson, D. O. and Dirmeyer, P. A.: Characterizing the Relationship between Temperature and Soil Moisture Extremes and Their Role in the Exacerbation of Heat Waves over the Contiguous United States, J. Clim., 34, 2175-2187, https://doi.org/10.1175/JCLI-D-20-0440.1, 2021.

Bian, Z., Li, H., Gottsche, F. M., Li, R., Du, Y., Ren, H., Cao, B., Xiao, Q., and Liu, Q.: Retrieving soil and vegetation temperatures from dual-angle and multipixel satellite observations, IEEE Journal of Selected Topics in Applied Earth Observations and Remote Sensing, 13, 5536-5549, 10.1109/jstars.2020.3024190, 2020.

Blyth, E. M., Arora, V. K., Clark, D. B., Dadson, S. J., De Kauwe, M. G., Lawrence, D. M., Melton, J. R., Pongratz, J., Turton, R. H., and Yoshimura, K.: Advances in land surface modelling, Current Climate Change Reports, 7, 45-71, 2021.

Cao, B., Wang, S., Hao, J., Sun, W., and Zhang, K.: Inconsistency and correction of manually observed ground surface temperatures over snow-covered regions, Agric. For. Meteorol., 338, 10.1016/j.agrformet.2023.109518, 2023.

Cheng, J., Liang, S., Yao, Y., and Zhang, X.: Estimating the optimal broadband emissivity spectral range for calculating surface longwave net radiation, IEEE Geoscience and Remote Sensing Letters, 10, 401-405, 2013.

Dorigo, W., Wagner, W., Albergel, C., Albrecht, F., Balsamo, G., Brocca, L., Chung, D., Ertl, M., Forkel, M., Gruber, A., Haas, E., Hamer, P. D., Hirschi, M., Ikonen, J., de Jeu, R., Kidd, R., Lahoz, W., Liu, Y. Y., Miralles, D., Mistelbauer, T., Nicolai-Shaw, N., Parinussa, R., Pratola, C., Reimer, C., van der Schalie, R., Seneviratne, S. I., Smolander, T., and Lecomte, P.: ESA CCI Soil Moisture for improved Earth system understanding: State-of-the art and future directions, Remote Sens. Environ., 203, 185-215, https://doi.org/10.1016/j.rse.2017.07.001, 2017.

Doughty, C. E., Keany, J. M., Wiebe, B. C., Rey-Sanchez, C., Carter, K. R., Middleby, K. B., Cheesman, A. W., Goulden, M. L., da Rocha, H. R., Miller, S. D., Malhi, Y., Fauset, S., Gloor, E., Slot, M., Oliveras Menor, I., Crous, K. Y., Goldsmith, G. R., and Fisher, J. B.: Tropical forests are approaching critical temperature thresholds, Nature, 621, 105-111, 10.1038/s41586-023-06391-z, 2023.

Duan, S.-B., Zhou, S., Li, Z.-L., Liu, X., Chang, S., Liu, M., Huang, C., Zhang, X., and Shang, G.: Improving monthly mean land surface temperature estimation by merging four products using the generalized three-cornered hat method and maximum likelihood estimation, Remote Sens. Environ., 302, 113989, https://doi.org/10.1016/j.rse.2023.113989, 2024.

Forzieri, G., Alkama, R., Miralles, D. G., and Cescatti, A.: Satellites reveal contrasting responses of regional climate to the widespread greening of Earth, Science, 356, 1180-1184, doi:10.1126/science.aal1727, 2017.

Garc á-Garc á, A., Cuesta-Valero, F. J., Miralles, D. G., Mahecha, M. D., Quaas, J., Reichstein, M., Zscheischler, J., and Peng, J.: Soil heat extremes can outpace air temperature extremes, Nat. Clim. Change, 10.1038/s41558-023-01812-3, 2023.

G ötsche, F.-M. and Olesen, F.-S.: Modelling the effect of optical thickness on diurnal cycles of land surface temperature, Remote Sens. Environ., 113, 2306-2316, 10.1016/j.rse.2009.06.006, 2009.

Gruber, A., Scanlon, T., van der Schalie, R., Wagner, W., and Dorigo, W.: Evolution of the ESA CCI Soil Moisture climate data records and their underlying merging methodology, Earth Syst. Sci. Data, 11, 717-739, 10.5194/essd-11-717-2019, 2019.

Gruber, A., Su, C. H., Zwieback, S., Crow, W., Dorigo, W., and Wagner, W.: Recent advances in (soil moisture) triple collocation analysis, International Journal of Applied Earth Observation and Geoinformation, 45, 200-211, https://doi.org/10.1016/j.jag.2015.09.002, 2016.

Gurung, T. R. and Chen, L.: Understanding the influence of soil moisture on heatwave characteristics in the contiguous United States, Environ. Res. Lett., 19, 064070, 10.1088/1748-9326/ad4dbb, 2024.

He, X., Liu, X., Ru, C., Deng, X., Zhao, R., and Yu, W.: Evaluating Spatial Representativeness Across Multiple Scales for a Comprehensive Ground Validation Network Using Landsat Land Surface Temperature Data and Random Forest, IEEE Trans. Geosci. Remote Sens., 63, 1-14, 10.1109/tgrs.2025.3570685, 2025.

Hu, H., Ye, B., Zhou, Y., and Tian, F.: A land surface model incorporated with soil freeze/thaw and its application in GAME/Tibet, Science in China Series D: Earth Sciences, 49, 1311-1322, 2006.

Jia, K., Liang, S., Liu, S., Li, Y., Xiao, Z., Yao, Y., Jiang, B., Zhao, X., Wang, X., Xu, S., and Cui, J.: Global Land Surface Fractional Vegetation Cover Estimation Using General Regression Neural Networks From MODIS Surface Reflectance, IEEE Trans. Geosci. Remote Sens., 53, 4787-4796, 10.1109/tgrs.2015.2409563, 2015.

https://doi.org/10.5194/essd-2025-682
Preprint. Discussion started: 9 March 2026

Jiang, K., Pan, Z., Pan, F., Teuling, A. J., Han, G., An, P., Chen, X., Wang, J., Song, Y., Cheng, L., Zhang, Z., Huang, N., Ma, S., Gao, R., Zhang, Z., Men, J., Lv, X., and Dong, Z.: Combined influence of soil moisture and atmospheric humidity on land surface temperature under different climatic background, iScience, 26, 106837, https://doi.org/10.1016/j.isci.2023.106837, 2023.

Jiang, Y., Tang, R., and Li, Z.-L.: A framework of correcting the angular effect of land surface temperature on evapotranspiration estimation in single-source energy balance models, Remote Sens. Environ., 283, 113306, https://doi.org/10.1016/j.rse.2022.113306, 2022.

Kong, Q. and Huber, M.: Regimes of soil moisture–wet-bulb temperature coupling with relevance to moist heat stress, J. Clim., 36, 7925-7942, 2023.

Lembrechts, J. J., van den Hoogen, J., Aalto, J., Ashcroft, M. B., De Frenne, P., Kemppinen, J., Kopecký, M., Luoto, M., Maclean, I. M. D., Crowther, T. W., Bailey, J. J., Haesen, S., Klinges, D. H., Niittynen, P., Scheffers, B. R., Van Meerbeek, K., Aartsma, P., Abdalaze, O., Abedi, M., Aerts, R., Ahmadian, N., Ahrends, A., Alatalo, J. M., Alexander, J. M., Allonsius, C. N., Altman, J., Ammann, C., Andres, C., Andrews, C., Ardö, J., Arriga, N., Arzac, A., Aschero, V., Assis, R. L., Assmann, J. J., Bader, M. Y., Bahalkeh, K., Barančok, P., Barrio, I. C., Barros, A., Barthel, M., Basham, E. W., Bauters, M., Bazzichetto, M., Marchesini, L. B., Bell, M. C., Benavides, J. C., Benito Alonso, J. L., Berauer, B. J., Bjerke, J. W., Björk, R. G., Björkman, M. P., Björnsdóttir, K., Blonder, B., Boeckx, P., Boike, J., Bokhorst, S., Brum, B. N. S., Brůna, J., Buchmann, N., Buysse, P., Camargo, J. L., Campoe, O. C., Candan, O., Canessa, R., Cannone, N., Carbognani, M., Carnicer, J., Casanova-Katny, A., Cesarz, S., Chojnicki, B., Choler, P., Chown, S. L., Cifuentes, E. F., Čiliak, M., Contador, T., Convey, P., Cooper, E. J., Cremonese, E., Curasi, S. R., Curtis, R., Cutini, M., Dahlberg, C. J., Daskalova, G. N., de Pablo, M. A., Della Chiesa, S., Dengler, J., Deronde, B., Descombes, P., Di Cecco, V., Di Musciano, M., Dick, J., Dimarco, R. D., Dolezal, J., Dorrepaal, E., Dušek, J., Eisenhauer, N., Eklundh, L., Erickson, T. E., Erschbamer, B., Eugster, W., Ewers, R. M., Exton, D. A., Fanin, N., Fazlioglu, F., Feigenwinter, I., Fenu, G., Ferlian, O., Fernández Calzado, M. R., Fernández-Pascual, E., Finckh, M., Higgens, R. F., Forte, T. a. G. W., Freeman, E. C., Frei, E. R., Fuentes-Lillo, E., García, R. A., García, M. B., Géron, C., Gharun, M., Ghosn, D., Gigauri, K., Gobin, A., Goded, I., Goeckede, M., Gottschall, F., Goulding, K., Govaert, S., Graae, B. J., Greenwood, S., Greiser, C., Grelle, A., Guénard, B., Guglielmin, M., Guillemot, J., Haase, P., Haider, S., Halbritter, A. H., Hamid, M., Hammerle, A., Hampe, A., Haugum, S. V., Hederová, L., Heinesch, B., Helfter, C., Hepenstrick, D., Herberich, M., Herbst, M., Hermanutz, L., Hik, D. S., Hoffrén, R., Homeier, J., Hörtnagl, L., Høye, T. T., Hrbacek, F., Hylander, K., Iwata, H., Jackowicz-Korczynski, M. A., Jactel, H., Järveoja, J., Jastrzębowski, S., Jentsch, A., Jiménez, J. J., Jónsdóttir, I. S., Jucker, T., Jump, A. S., Juszczak, R., Kanka, R., Kašpar, V., Kazakis, G., Kelly, J., Khuroo, A. A., Klemedtsson, L., Klisz, M., Kljun, N., Knohl, A., Kobler, J., Kollár, J., Kotowska, M. M., Kovács, B., Kreyling, J., Lamprecht, A., Lang, S. I., Larson, C., Larson, K., Laska, K., le Maire, G., Leihy, R. I., Lens, L., Liljebladh, B., Lohila, A., Lorite, J., Loubet, B., Lynn, J., Macek, M., Mackenzie, R., Magliulo, E., Maier, R., Malfasi, F., Máliš, F., Man, M., Manca, G., Manco, A., Manise, T., Manolaki, P., Marciniak, F., Matula, R., Mazzolari, A. C., Medinets, S., Medinets, V., Meeussen, C., Merinero, S., Mesquita, R. d. C. G., Meusburger, K., Meysman, F. J. R., Michaletz, S. T., Milbau, A., Moiseev, D.,

https://doi.org/10.5194/essd-2025-682
Preprint. Discussion started: 9 March 2026

Moiseev, P., Mondoni, A., Monfries, R., Montagnani, L., Moriana-Armendariz, M., Morra di Cella, U., Mörsdorf, M., Mosedale, J. R., Muffler, L., Muñoz-Rojas, M., Myers, J. A., Myers-Smith, I. H., Nagy, L., Nardino, M., Naujokaitis-Lewis, I., Newling, E., Nicklas, L., Niedrist, G., Niessner, A., Nilsson, M. B., Normand, S., Nosetto, M. D., Nouvellon, Y., Nuñez, M. A., Ogaya, R., Ogée, J., Okello, J., Olejnik, J., Olesen, J. E., Opedal, Ø. H., Orsenigo, S., Palaj, A., Pampuch, T., Panov, A. V., Pärtel, M., Pastor, A., Pauchard, A., Pauli, H., Pavelka, M., Pearse, W. D., Peichl, M., Pellissier, L., Penczykowski, R. M., Penuelas, J., Petit Bon, M., Petraglia, A., Phartyal, S. S., Phoenix, G. K., Pio, C., Pitacco, A., Pitteloud, C., Plichta, R., Porro, F., Portillo-Estrada, M., Poulenard, J., Poyatos, R., Prokushkin, A. S., Puchalka, R., Puşcaş, M., Radujković, D., Randall, K., Ratier Backes, A., Remmele, S., Remmers, W., Renault, D., Risch, A. C., Rixen, C., Robinson, S. A., Robroek, B. J. M., Rocha, A. V., Rossi, C., Rossi, G., Roupsard, O., Rubtsov, A. V., Saccone, P., Sagot, C., Sallo Bravo, J., Santos, C. C., Sarneel, J. M., Scharnweber, T., Schmeddes, J., Schmidt, M., Scholten, T., Schuchardt, M., Schwartz, N., Scott, T., Seeber, J., Segalin de Andrade, A. C., Seipel, T., Semenchuk, P., Senior, R. A., Serra-Diaz, J. M., Sewerniak, P., Shekhar, A., Sidenko, N. V., Siebicke, L., Siegwart Collier, L., Simpson, E., Siqueira, D. P., Sitková, Z., Six, J., Smiljanic, M., Smith, S. W., Smith-Tripp, S., Somers, B., Sørensen, M. V., Souza, J. J. L. L., Souza, B. I., Souza Dias, A., Spasojevic, M. J., Speed, J. D. M., Spicher, F., Stanisci, A., Steinbauer, K., Steinbrecher, R., Steinwandter, M., Stemkovski, M., Stephan, J. G., Stiegler, C., Stoll, S., Svátek, M., Svoboda, M., Tagesson, T., Tanentzap, A. J., Tanneberger, F., Theurillat, J.-P., Thomas, H. J. D., Thomas, A. D., Tielbörger, K., Tomaselli, M., Treier, U. A., Trouillier, M., Turtureanu, P. D., Tutton, R., Tyystjärvi, V. A., Ueyama, M., Ujházy, K., Ujházyová, M., Uogintas, D., Urban, A. V., Urban, J., Urbaniak, M., Ursu, T.-M., Vaccari, F. P., Van de Vondel, S., van den Brink, L., Van Geel, M., Vandvik, V., Vangansbeke, P., Varlagin, A., Veen, G. F., Veenendaal, E., Venn, S. E., Verbeeck, H., Verbrugggen, E., Verheijen, F. G. A., Villar, L., Vitale, L., Vittoz, P., Vives-Ingla, M., von Oppen, J., Walz, J., Wang, R., Wang, Y., Way, R. G., Wedegärtner, R. E. M., Weigel, R., Wild, J., Wilkinson, M., Wilmking, M., Wingate, L., Winkler, M., Wipf, S., Wohlfahrt, G., Xenakis, G., Yang, Y., Yu, Z., Yu, K., Zellweger, F., Zhang, J., Zhang, Z., Zhao, P., Ziemblińska, K., Zimmermann, R., Zong, S., Zyryanov, V. I., Nijs, I., and Lenoir, J.: Global maps of soil temperature, Glob. change biol., 28, 3110-3144, https://doi.org/10.1111/gcb.16060, 2022.

Li, J., Li, Z.-L., Wu, H., and You, N.: Trend, seasonality, and abrupt change detection method for land surface temperature time-series analysis: Evaluation and improvement, Remote Sens. Environ., 280, 113222, https://doi.org/10.1016/j.rse.2022.113222, 2022.

Li, X. and Xiao, J.: A Global, 0.05-Degree Product of Solar-Induced Chlorophyll Fluorescence Derived from OCO-2, MODIS, and Reanalysis Data, Remote Sens., 11, 517, 2019.

Li, Z.-L., MP, S., Zhang, R., Jia, L., and Su, Z.: On the separate retrieval of soil and vegetation temperatures from ATSR data, Science in China Series D: Earth Sciences, 44, 97, 2001.

Li, Z.-L., Leng, P., Zhou, C., Chen, K.-S., Zhou, F.-C., and Shang, G.-F.: Soil moisture retrieval from remote sensing measurements: Current knowledge and directions for the future, Earth-Science Reviews, 218, 10.1016/j.earscirev.2021.103673, 2021.

Li, Z.-L., Tang, B.-H., Wu, H., Ren, H., Yan, G., Wan, Z., Trigo, I. F., and Sobrino, J. A.: Satellite-derived land surface temperature: Current status and perspectives, Remote Sens. Environ., 131, 14-37, https://doi.org/10.1016/j.rse.2012.12.008, 2013.

Li, Z.-L., Wu, H., Duan, S.-B., Zhao, W., Ren, H., Liu, X., Leng, P., Tang, R., Ye, X., Zhu, J., Sun, Y., Si, M., Liu, M., Li, J., Zhang, X., Shang, G., Tang, B.-H., Yan, G., and Zhou, C.: Satellite Remote Sensing of Global Land Surface Temperature: Definition, Methods, Products, and Applications, Reviews of Geophysics, 61, e2022RG000777, https://doi.org/10.1029/2022RG000777, 2023.

Liu, X. and Li, Z.-L.: GloSVeT: a global 0.05 ° monthly mean surface soil and vegetation component temperature dataset (2003-2023) [Data set]. Zenodo. https://doi.org/10.5281/zenodo.17461084, 2025.

Liu, X. and Li, Z.-L.: GloSVeT: a global 0.05 ° monthly mean surface soil and vegetation component temperature dataset (2003-2023) [Data set]. National Tibetan Plateau / Third Pole Environment Data Center. https://doi.org/10.11888/, 2026.

Liu, X., Li, Z.-L., Duan, S.-B., Leng, P., and Si, M.: Retrieval of global surface soil and vegetation temperatures based on multisource data fusion, Remote Sens. Environ., 318, 10.1016/j.rse.2024.114564, 2025.

Liu, X., Tang, B.-H., Li, Z.-L., Zhang, X., and Shang, G.: On the Derivation of Geometric Optical Kernels for Directional Thermal Radiation, Earth and Space Science, 7, e2019EA000895, 10.1029/2019EA000895, 2020a.

Liu, X., Li, Z.-L., Li, J.-H., Leng, P., Liu, M., and Gao, M.: Temporal upscaling of MODIS 1-km instantaneous land surface temperature to monthly mean value: Method evaluation and product generation, IEEE Trans. Geosci. Remote Sens., 5001214, 10.1109/TGRS.2023.3247428, 2023.

Liu, X., Tang, B.-H., Li, Z.-L., Zhou, C., Wu, W., and Rasmussen, M. O.: An improved method for separating soil and vegetation component temperatures based on diurnal temperature cycle model and spatial correlation, Remote Sens. Environ., 248, 111979, 10.1016/j.rse.2020.111979, 2020b.

Lu, Y., Bian, Z., Roujean, J.-L., Li, H., Göttsche, F. M., Huang, Y., Fan, T., Cao, B., Du, Y., and Xiao, Q.: Improved satellite-scale land surface temperature components retrieval with hotspot effect correction and temperature difference constraints, Remote Sens. Environ., 326, 10.1016/j.rse.2025.114794, 2025.

Luan, X. and Vico, G.: Canopy temperature and heat stress are increased by compound high air temperature and water stress and reduced by irrigation – a modeling analysis, Hydrol. Earth Syst. Sci., 25, 1411-1423, 10.5194/hess-25-1411-2021, 2021.

Lundquist, J. D., Chickadel, C., Cristea, N., Currier, W. R., Henn, B., Keenan, E., and Dozier, J.: Separating snow and forest temperatures with thermal infrared remote sensing, Remote Sens. Environ., 209, 764-779, 10.1016/j.rse.2018.03.001, 2018.

Ma, Y., Zhou, J., Liu, S., Zhang, W., Zhang, Y., Xu, Z., Song, L., and Zhao, H.: Estimation of evapotranspiration using all-weather land surface temperature and variational trends with warming temperatures for the River Source Region in Southwest China, Journal of Hydrology, 613, 128346, https://doi.org/10.1016/j.jhydrol.2022.128346, 2022.

Manzoni, S., Chakrawal, A., Fischer, T., Schimel, J. P., Porporato, A., and Vico, G.: Rainfall intensification increases the contribution of rewetting pulses to soil heterotrophic respiration, Biogeosciences, 17, 4007-4023, 10.5194/bg-17-4007-2020, 2020.

https://doi.org/10.5194/essd-2025-682
Preprint. Discussion started: 9 March 2026

Muñoz-Sabater, J., Dutra, E., Agustí-Panareda, A., Albergel, C., Arduini, G., Balsamo, G., Boussetta, S., Choulga, M., Harrigan, S., Hersbach, H., Martens, B., Miralles, D. G., Piles, M., Rodríguez-Fernández, N. J., Zsoter, E., Buontempo, C., and Thépaut, J. N.: ERA5-Land: a state-of-the-art global reanalysis dataset for land applications, Earth Syst. Sci. Data, 13, 4349-4383, 10.5194/essd-13-4349-2021, 2021.

Pan, L., Xiao, X., Yao, Y., Pan, B., Yin, C., Meng, C., Qin, Y., and Zhang, C.: Site-specific apparent optimum air temperature for vegetation photosynthesis across the globe, Scientific Data, 11, 758, 10.1038/s41597-024-03603-7, 2024.

Park, J., Baik, J., and Choi, M.: Triple collocation-based multi-source evaporation and transpiration merging, Agric. For. Meteorol., 331, 109353, 2023.

Pelikan, M.: Bayesian Optimization Algorithm, in: Hierarchical Bayesian Optimization Algorithm: Toward a new Generation of Evolutionary Algorithms, edited by: Pelikan, M., Springer Berlin Heidelberg, Berlin, Heidelberg, 31-48, 10.1007/978-3-540-32373-0_3, 2005.

Premoli, A. and Tavella, P.: A revisited three-cornered hat method for estimating frequency standard instability, IEEE Transactions on instrumentation and measurement, 42, 7-13, 1993.

Prentice, I. C., Balzarolo, M., Bloomfield, K. J., Chen, J. M., Dechant, B., Ghent, D., Janssens, I. A., Luo, X., Morfopoulos, C., Ryu, Y., Vicca, S., and van Hoolst, R.: Principles for satellite monitoring of vegetation carbon uptake, Nature Reviews Earth & Environment, 5, 818-832, 10.1038/s43017-024-00601-6, 2024.

Qiao, L., Zuo, Z., Zhang, R., Piao, S., Xiao, D., and Zhang, K.: Soil moisture–atmosphere coupling accelerates global warming, Nat. Commun., 14, 4908, 10.1038/s41467-023-40641-y, 2023.

Qiao, L., Zuo, Z., Zhang, R., Mei, W., Chen, D., Chang, M., and Zhang, K.: Extreme Dry-Hot in North America and Europe: The Amplified Role of Warming-Enhanced Land-Air Coupling, National Science Review, nwaf435, 10.1093/nsr/nwaf435, 2025.

Rodell, M., Houser, P., Jambor, U., Gottschalck, J., Mitchell, K., Meng, C.-J., Arsenault, K., Cosgrove, B., Radakovich, J., and Bosilovich, M.: The global land data assimilation system, Bulletin of the American Meteorological society, 85, 381-394, 2004.

Rutter, N., Essery, R., Baxter, R., Hancock, S., Horton, M., Huntley, B., Reid, T., and Woodward, J.: Canopy Structure and Air Temperature Inversions Impact Simulation of Sub-Canopy Longwave Radiation in Snow-Covered Boreal Forests, J. Geophys. Res. Atmos., 128, e2022JD037980, https://doi.org/10.1029/2022JD037980, 2023.

Seneviratne, S. I., Corti, T., Davin, E. L., Hirschi, M., Jaeger, E. B., Lehner, I., Orlowsky, B., and Teuling, A. J.: Investigating soil moisture–climate interactions in a changing climate: A review, Earth-Science Reviews, 99, 125-161, https://doi.org/10.1016/j.earscirev.2010.02.004, 2010.

Sims, D. A., Rahman, A. F., Cordova, V. D., El-Masri, B. Z., Baldocchi, D. D., Bolstad, P. V., Flanagan, L. B., Goldstein, A. H., Hollinger, D. Y., and Misson, L.: A new model of gross primary productivity for North American ecosystems based solely on the enhanced vegetation index and land surface temperature from MODIS, Remote Sens. Environ., 112, 1633-1646, 2008.

https://doi.org/10.5194/essd-2025-682
Preprint. Discussion started: 9 March 2026

Sjoberg, J. P., Anthes, R. A., and Rieckh, T.: The three-cornered hat method for estimating error variances of three or more atmospheric datasets. Part I: overview and evaluation, J. Atmos. Ocean. Technol., 38, 555-572, 2021.

Song, L., Liu, S., Kustas, W., Zhou, J., and Ma, Y.: Using the surface temperature-albedo space to separate regional soil and vegetation temperatures from ASTER data, Remote Sens., 7, 5828-5848, 10.3390/rs70505828, 2015.

Song, L., Bian, Z., Kustas, W. P., Liu, S., Xiao, Q., Nieto, H., Xu, Z., Yang, Y., Xu, T., and Han, X.: Estimation of surface heat fluxes using multi-angular observations of radiative surface temperature, Remote Sens. Environ., 239, 111674, https://doi.org/10.1016/j.rse.2020.111674, 2020.

Stoffelen, A.: Toward the true near-surface wind speed: Error modeling and calibration using triple collocation, Journal of geophysical research: oceans, 103, 7755-7766, 1998.

Sulla-Menashe, D., Gray, J. M., Abercrombie, S. P., and Friedl, M. A.: Hierarchical mapping of annual global land cover 2001 to present: The MODIS Collection 6 Land Cover product, Remote Sens. Environ., 222, 183-194, 2019.

Tang, Y., Xu, X., Zhou, Z., Qu, Y., and Sun, Y.: Estimating global maximum gross primary productivity of vegetation based on the combination of MODIS greenness and temperature data, Ecological Informatics, 63, 101307, 2021.

Trew, B. T., Edwards, D. P., Lees, A. C., Klinges, D. H., Early, R., Sváteк, M., Plichta, R., Matula, R., Okello, J., Niessner, A., Barthel, M., Six, J., Maeda, E. E., Barlow, J., do Nascimento, R. O., Berenguer, E., Ferreira, J., Sallo-Bravo, J., and Maclean, I. M. D.: Novel temperatures are already widespread beneath the world's tropical forest canopies, Nat. Clim. Change, 14, 753-759, 10.1038/s41558-024-02031-0, 2024.

Wan, W., Liu, Z., Li, K., Wang, G., Wu, H., and Wang, Q.: Drought monitoring of the maize planting areas in Northeast and North China Plain, Agricultural Water Management, 245, 106636, 2021.

Wan, Z. and Dozier, J.: A generalized split-window algorithm for retrieving land-surface temperature from space, IEEE Trans. Geosci. Remote Sens., 34, 892-905, 10.1109/36.508406, 1996.

Wan, Z. and Li, Z.-L.: A physics-based algorithm for retrieving land-surface emissivity and temperature from EOS/MODIS data, IEEE Trans. Geosci. Remote Sens., 35, 980-996, 10.1109/36.602541, 1997.

Wang, S., Zhan, W., Zhou, B., Tong, S., Chakraborty, T., Wang, Z., Huang, K., Du, H., Middel, A., and Li, J.: Dual impact of global urban overheating on mortality, Nat. Clim. Change, 1-8, 2025.

Wei, L., Jiang, S., Dong, J., Ren, L., Yong, B., Yang, B., Li, X., and Duan, Z.: A combined extended triple collocation and cumulative distribution function merging framework for improved daily precipitation estimates over mainland China, Journal of Hydrology, 641, 131757, 2024.

Williams, C., McNamara, J., and Chandler, D.: Controls on the temporal and spatial variability of soil moisture in a mountainous landscape: the signature of snow and complex terrain, Hydrology and Earth System Sciences, 13, 1325-1336, 2009.

Xing, Z., Li, Z.-L., Duan, S.-B., Liu, X., Zheng, X., Leng, P., Gao, M., Zhang, X., and Shang, G.: Estimation of daily mean land surface temperature at global scale using pairs of daytime and nighttime MODIS instantaneous observations, ISPRS J. Photogramm. Remote Sens., 178, 51-67, 10.1016/j.isprsjprs.2021.05.017, 2021.

https://doi.org/10.5194/essd-2025-682
Preprint. Discussion started: 9 March 2026

Yu, X., Xu, X., Zhan, L., Cheng, H., and Xin, P.: Seasonal Temperature Distributions and Variations in Salt Marshes: Field Investigation and Numerical Simulation, Water Resources Research, 60, e2023WR037016, https://doi.org/10.1029/2023WR037016, 2024.

Zhan, W., Chen, Y., Zhou, J., and Li, J.: An algorithm for separating soil and vegetation temperatures with sensors featuring a single thermal channel, IEEE Trans. Geosci. Remote Sens., 49, 1796-1809, 2011.

Zhan, W., Chen, Y., Zhou, J., Wang, J., Liu, W., Voogt, J., Zhu, X., Quan, J., and Li, J.: Disaggregation of remotely sensed land surface temperature: Literature survey, taxonomy, issues, and caveats, Remote Sens. Environ., 131, 119-139, 10.1016/j.rse.2012.12.014, 2013.

Zhang, P., Zheng, D., van der Velde, R., Wen, J., Ma, Y., Zeng, Y., Wang, X., Wang, Z., Chen, J., and Su, Z.: A dataset of 10-year regional-scale soil moisture and soil temperature measurements at multiple depths on the Tibetan Plateau, Earth Syst. Sci. Data, 14, 5513-5542, 10.5194/essd-14-5513-2022, 2022.

Zhao, E., Qu, N., Wang, Y., Gao, C., and Zeng, J.: TEBS: Temperature–Emissivity–Driven band selection for thermal infrared hyperspectral image classification with structured State-Space model and gated attention, International Journal of Applied Earth Observation and Geoinformation, 142, 104710, https://doi.org/10.1016/j.jag.2025.104710, 2025.

Zhao, W., Li, A., Bian, J., Jin, H., and Zhang, Z.: A synergetic algorithm for mid-morning land surface soil and vegetation temperatures estimation using MSG-SEVIRI products and TERRA-MODIS products, Remote Sens., 6, 2213-2238, 2014.

Zhao, Z., De Frenne, P., Peñuelas, J., Van Meerbeek, K., Fornara, D. A., Peng, Y., Wu, Q., Ni, X., Wu, F., and Yue, K.: Effects of snow cover-induced microclimate warming on soil physicochemical and biotic properties, Geoderma, 423, 115983, 2022.